SCIENCE CHINA
Earth Sciences

•RESEARCH PAPER•

March 2019 Vol.62 No.3: 529–549
https://doi.org/10.1007/s11430-018-9286-6

Structural architecture of Neoproterozoic rifting depression groups in the Tarim Basin and their formation dynamics

Bizhu HE[1*], Cunli JIAO[2], Taizhu HUANG[3], Xingui ZHOU[4], Zhihui CAI[1], Zicheng CAO[3], Zhongzheng JIANG[3], Junwen CUI[1], Zhuoyin YU[1], Weiwei CHEN[1], Ruohan LIU[1], Xiaorui YUN[1] & Guangming HAO[1]

[1] *Institute of Geology, Chinese Academy of Geological Sciences, Beijing 100037, China;*
[2] *Exploration and Production Research Institute of SINOPEC, Beijing 100083, China;*
[3] *Institute of Northwestern Petroleum Subsidiary of SINOPEC, Urumqi 830011, China;*
[4] *Oil and Gas Investigation Centre of China Geological Survey, Beijing 100029, China*

Received January 16, 2018; revised September 20, 2018; accepted October 18, 2018; published online January 15, 2019

Abstract The Tarim Basin is the largest, oil-bearing, superimposed basin in the northwest of China. The evolution and tectonic properties of the initial Tarim Basin have been hotly disputed and remain enigmatic. The Neoproterozoic basin is covered by a vast desert and a huge-thickness of sedimentary strata, has experienced multiple tectonic movements, had a low signal to noise ratios (SNRs) of deep seismic reflection data, all of which have posed critical obstacles to research. We analysed four field outcrops, 18 wells distributed throughout the basin, 27 reprocessed seismic reflection profiles with higher SNRs across the basin and many ancillary local 2D and 3D profiles and aeromagnetic data. We found about 20 normal fault-controlled rifting depressions of the Cryogenian and Ediacaran scattered throughout the basin, which developed on the Precambrian metamorphic and crystalline basement. The structural framework is clearly different from that of the overlying Phanerozoic. The rifting depressions consist of mainly half grabens, symmetrical troughs and horst-grabens. From the northeast to southwest of the basin, they are divided into three rifting depression groups with the WNW, ENE, and NW-trends that are mainly controlled by normal faults. The maximum thicknesses of the strata are up to 4100 m. From the Cryogenian to Ediacaran, most of the main inherited faults to active and eventually ceased at the end of the Ediacaran or Early Cambrian, while subsidence centres appeared and migrated eastward along the faults. They revealed that the different parts of the Tarim continental block were in NNE-SSW-oriented and NNW-SSE-oriented extensional paleo-stress fields (relative to the present) during the Neoproterozoic, and were accompanied by clockwise shearing. According to the analysis of the activities of syn-sedimentary faults, filling sediments, magmatic events, and coordination with aeromagnetic anomalies, the tectonic properties of the fault depressions are different and are primarily continental rifts or intra-continental fault-controlled basins. The rifting phases mainly occurred from 0.8–0.61 Ga. The formation of the rifting depression was associated with the initial opening of the South Altun-West Kunlun Ocean and the South Tianshan Ocean, which were located at the northern and southern margins of the Tarim Block, respectively, in response to the break-up of the Supercontinent Rodinia and the initial opening of the Proto-Tethys Ocean.

Keywords Rifting depression groups, Normal faults, Extensional and clockwise shearing, Cryogenian and Ediacaran, Continental rift and intra-continental fault-controlled basin, Tarim Basin

Citation: He B, Jiao C, Huang T, Zhou X, Cai Z, Cao Z, Jiang Z, Cui J, Yu Z, Chen W, Liu R, Yun X, Hao G. 2019. Structural architecture of Neoproterozoic rifting depression groups in the Tarim Basin and their formation dynamics. Science China Earth Sciences, 62: 529–549, https://doi.org/10.1007/s11430-018-9286-6

* Corresponding author (email: hebizhu@cags.ac.cn; hebizhu@vip.sina.com)

1. Introduction

The Tarim Basin is the largest hydrocarbon-bearing superimposed basin in northwestern China (Xiao et al., 1990; He and Li, 1996; Jia, 2004; Xu Z Q et al., 2013), with an area of 56×10^4 km^2, which contains both marine and terrestrial sedimentary rocks and was developed on Precambrian metamorphic basement. It is bordered by the Tianshan-Beishan, Altun and West Kunlun orogenic belts, while most of the surface of the basin is occupied by Takelamagan desert. Studies on the Phanerozoic tectonic evolution and energy resource explorations of the Tarim Basin and its peripheral orogens have made significant achievements (Jia, 2009; Kang, 2012).

However, the properties and structures of the Neoproterozoic and the initial Tarim Basin are still controversial. Different definitions of the initial basin include an aulacogen (Jia, 1997; Jia, 2004), a continental rift basin (Xu et al., 2005, 2009; Zhang et al., 2016), a foreland basin-passive continental margin (Zhu et al., 2011; Zhang et al., 2016), and a continental back-arc sedimentary basin (Zhang Y L et al., 2013), etc (Figure 1). The distribution of the Neoproterozoic strata in the Tarim Basin has also been described differently, such as in the northern depression (Jia, 2004), or both in the northern depression and in the southwest of the basin, but is missing in the Central Uplift Zone (Zhou et al., 2015; Wu et al., 2016). At the Keping faulted-uplift, the Kuluktage area, the Altun Mountain and north of the West Kunlun Mountain, there are obvious differences in the strata types of the Neoproterozoic, the contacts between the basement and initial sedimentary layers, the thicknesses and types of sedimentary rocks, and the tectonism and transformation. Therefore, the structural attributes, stratigraphic distribution, sedimentary development and tectonic evolution and formation geodynamics of the Neoproterozoic in the Tarim Basin are key points of study that present difficult problems.

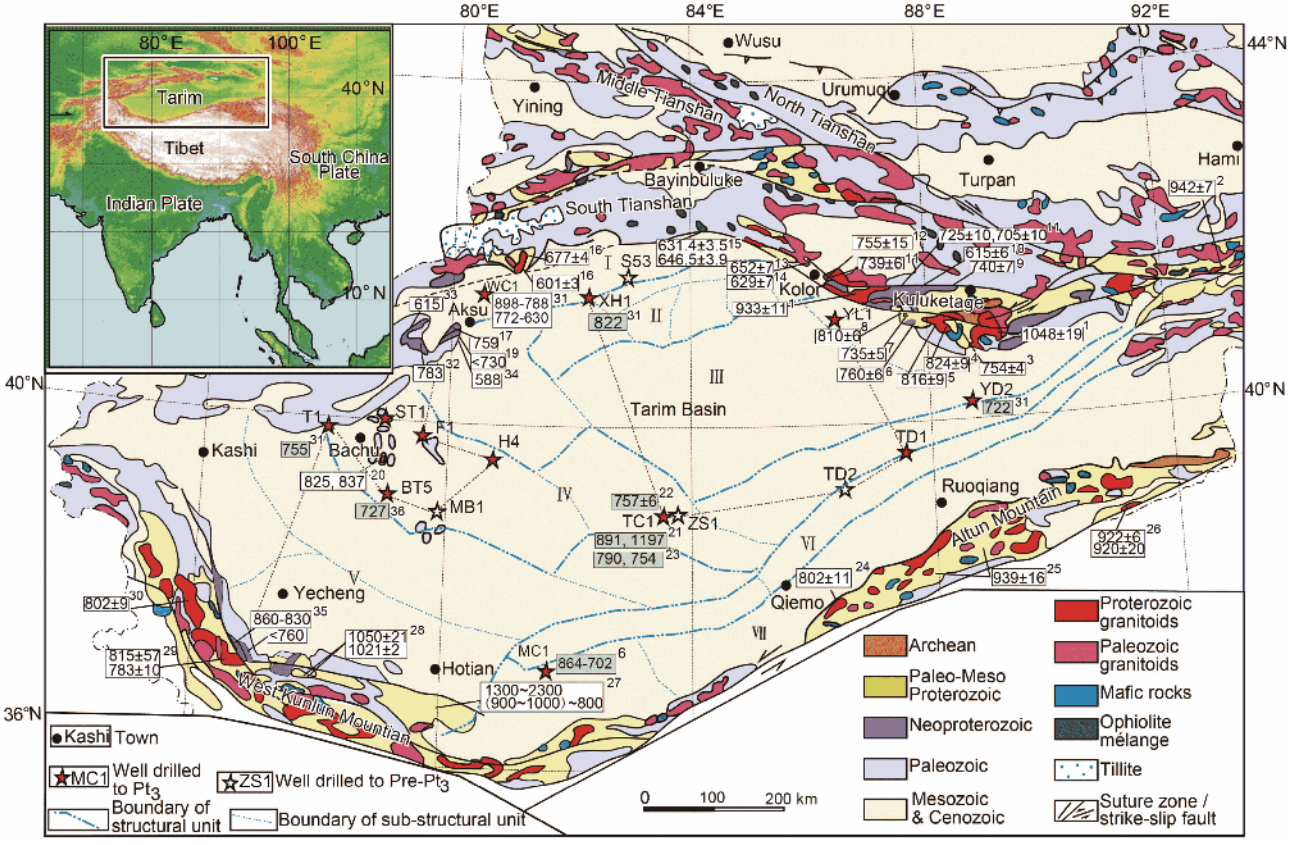

Figure 1 A schematic map of the structural units at present, and metamorphic and magmatic events during the Neoproterozoic in the Tarim Basin and its adjacent areas (modified from Bureau of Geology and Mineral Resources of Xinjiang Uygur Autonomous region, 1993; Xu et al., 2011, 2013; Zhang et al., 2011; Zhang et al., 2012b, 2016; Ge et al., 2012). The digits in the boxes are the age data in Ma. The black dotted lines are the stratigraphic correlation profiles from the outcrops to the deep drillholes in the basin, as shown in Figures 2 and 3. Structural units of Tarim Basin in the Phanerozoic: I, Kuqa Depression; II, Tabei (North) Uplift; III, North Depression Zone; IV, Central Uplift Zone; V, Southwest Depression Zone; VI, Dongnan (Southeast) Faulted Uplift; and VII, Dongnan (Southeast) Depression. References of the Neoproterozoic ages: 1, Shu et al. (2011); 2, Hu et al. (2010); 3, Long et al. (2011); 4, Zhang et al. (2007a); 5, Deng et al. (2008); 6, Zhang et al. (2012a); 7, Zhang et al. (2006); 8, Zhang et al. (2007b); 9, 10, Xu et al. (2009); 11, Gao et al. (2010); 12, Xu et al. (2005); 13, Zhu et al. (2008); 14, Luo et al. (2016); 15, He D F et al. (2011); 16, Wei et al. (2010); 17, Zhang et al. (2009); 19, Zhu et al. (2011); 20, Li et al. (1999); 21, Li et al. (2005); 22, Wu et al. (2009); 23, Guo et al. (2005); 24, 25, Zhang et al. (2011); 26, Gehrels et al. (2003a); 27, Zhang et al. (2007a); 28, Zhang et al. (2003); 29, Zhang et al. (2006); 30, Zhang et al. (2010); 31, Xu Z Q et al. (2013); 32, Zhang Z C et al. (2012); 33, Xu B et al. (2013); 34, He et al. (2014); 35, Zhang et al. (2016); 36, this paper.

In this study, by utilizing the peripheral outcrop sections, drilling and logging data, 2-D seismic data in basin-scale and many local 2-D and 3-D seismic data and aeromagnetic data, we carried out a study of the deep-buried structure—sedimentation systems—of the Neoproterozoic Tarim Basin, established the tectonic framework and analysed the fine structural architecture of the Neoproterozoic, explained the spatial distribution and palaeotectonic properties and discussed the formation dynamics of the basin. This study provides new data for deep hydrocarbon exploration in the Tarim Basin, and also provides new evidence for unravelling the process of initiation of cratonic sedimentary basins.

2. Geological setting

2.1 The basement framework of the Tarim Basin

The Tarim Block experienced an initial stage of continental crust evolution during the Archaean (Bureau of Geology and Mineral Resources of Xinjiang Uygur Autonomous region, 1993; Lu et al., 2006, 2008; Long et al., 2010, 2011; Zhang et al., 2012a) and the orogenic events during the end of the Paleoproterozoic to the late Mesoproterozoic and early Neoproterozoic (Zhang J X et al., 2012; Zhu et al., 2008) eventually formed the Precambrian basement of the Tarim Basin. The development and evolution of Tarim Block are closely related to the convergence of the Supercontinent Columbia during 2.0 Ga to 1.8 Ga (Rogers and Santosh, 2002; Zhao et al., 2002, 2004, 2012; Zhai and Santosh, 2011; Santosh et al., 2009) and the Supercontinent Rodinia at ca. 1.0 Ga (Li Z X et al., 2003, 2008, 2013; Li et al., 2005; Li and Zhong, 2009).

A three-fold subdivision of the Presinian basement of the Tarim Block was suggested (Xu Z Q et al., 2013). The North Tarim Block, including the northern part of the Tarim Basin, the Korla-Kuluktage area and the Dunhuang area, possesses a ca. 2.7–2.5 Ga or an even older aged continental nucleus (Long et al., 2010, Zhang et al., 2012a, Xu Z Q et al., 2013). The block underwent multiple phases of magmatic and metamorphic events at ca. 2.0–1.8 Ga, 1.0–0.8 Ga and 760–687 Ma (Xu et al., 2005, 2009; Xu Z Q et al., 2013; Zhu et al., 2008, 2011, 2017). The Central Tarim Tectonic Belt, which encompasses the Precambrian basement of the central part of the Tarim Basin and the Altun Orogenic Belt, are characterized by a magmatic island arc system during 940–890 Ma (Li Y J et al., 2003; Wu et al., 2006), but there is still a lack of sufficient evidence on how it extends from the eastern Altun terrane to the basin (Guo et al., 1999; Zhang et al., 2011; Xu Z Q et al., 2013). The South Tarim Block, with a 2.4–2.3 Ga aged continental nucleus, contains the Precambrian basement of the southern part of the Tarim Basin, western Kunlun and parts of the eastern Kunlun Orogenic belt, and underwent 2.0–1.75 Ga and 1.0–0.8 Ga metamorphic and magmatic events (Zhang et al., 2007c, 2012b).

The Neoproterozoic in the Tarim Basin developed on different Precambrian basement. The Precambrian basement contains: (1) Neoarchean magmatic complexes dominated by TTG rocks (Bureau of Geology and Mineral Resources of Xinjiang Uygur Autonomous region, 1993; Lu et al., 2008; Long et al., 2010; Zhang et al., 2012b); (2) Paleoproterozoic metamorphic rocks (Zhang C L et al., 2003; Long et al., 2011; Zhang J X et al., 2013); and (3) the Mesoproterozoic-early Neoproterozoic metamorphic rocks containing greenschists (Zhang et al., 2005a; Shu et al., 2011).

2.2 Initial sedimentary filling of the Tarim Basin

Neoproterozoic sedimentary rocks in the peripheral outcrops of the Tarim Basin comprise a large thickness of various sedimentary types, and are dominated by terrestrial and glacial deposition in the early stages, with marine deposition in the later stages; and contain 2–4 sets of tillites (Gao et al., 1993; Jia et al., 2004; He et al., 2007; Gao et al., 2010, 2013) and several igneous rock layers (Xu B et al., 2005, 2013; Zhang et al., 2007c; Wang et al., 2010; Zhang Z C et al., 2012, 2016). The lower unit of the Neoproterozoic directly overlies the metamorphic and magmatic Precambrian basement of the basin. A regional angular or parallel unconformity separates the upper Neoproterozoic and the lower Cambrian sequences (Qian et al., 2014; Kang et al., 2016). However, the sedimentary sequences of the Neoproterozoic are relatively complex. Up to now, 18 deep boreholes have been drilled into the Neoproterozoic or Precambrian basement in the Tarim Basin. Most of them are mainly distributed on the uplifts of the structural units in the basin, and several of the drillholes are missing the Cryogenian and the Ediacaran (equivalent of the Nanhuaian and Sinian systems in the Chinese Geological Timescale) of the Neoproterozoic (Xu Z Q et al., 2013; Wu et al., 2016). Some of them are even missing the important source rocks of the lower Cambrian Yurtusi Formation (Fm.) (Jia et al., 2004; Zhang G Y et al., 2015). Carbonate rocks of the Xorbulak Formation directly overly the Paleoproterozoic basement (Xu Z Q et al., 2013).

Despite some drillhole data, the Neoproterozoic of the Tarim Basin has received a low level of exploration and research. Therefore, there is no unified comparative standard for the stratigraphy in the basin and the adjacent peripheral orogenic belts, which needs to be further studied.

3. Stratigraphic characters of the Neoproterozoic

The earliest sedimentary cover in the Kuluktage area on the northeast margin of the Tarim Basin consists mainly of the Kuluktage Group (Gr.) of the Neoproterozoic. It is preserved

the most complete Neoproterozoic strata in the Tarim Basin. The Neoproterozoic in the Kuluktage area is composed of the Tonian (corresponds to the Qingbaikouian), Cryogenian (Nanhuaian) and Ediacaran (Sinian) in ascending order, and it can be further divided into ten formations (Gao et al., 1993). The Neoproterozoic, which is up to 6000 m thick (Figures 1 and 2), is dominated by littoral and marine sedimentary rocks intercalated with volcanic rocks. There are four sets of tillites and 3 phases of the magmatic events (Xu et al., 2005, 2009; Gao et al., 2010; Zhu et al., 2011; He et al., 2012). The metamorphic basement consists mainly of the Tuoge Complex of the Neoarchean-Paleoproterozoic or older ages and the Xingditage Group of the Mesoproterozoic–early Neoproterozoic (Bureau of Geology and Mineral Resources of Xinjiang Uygur Autonomous region, 1993; Lu and Yuan, 2003; Hu and Wei, 2006; Lu et al., 2008). These underwent two metamorphic events around 2.0–1.8 and 1.1–1.0 Ga (Long et al., 2011; Shu et al., 2011; Zhang et al., 2012a).

The first set of sedimentary cover in the Aksu area on the northwest margin of the Tarim Basin is the Neoproterozoic with an unconformity overlying the Aksu Group. The strata are composed of Qiaoenbrak and Yourmeinak formations of the Cryogenian and Sugetbrak and Chigebrak formations of the Ediacaran in ascending order (Gao and Zhu, 1984; Jia, 2004). The lower Neoproterozoic is characterized by terrestrial brown-red conglomerates and sandstones, and a transition upward to marine sandstones, glacial turbidites and

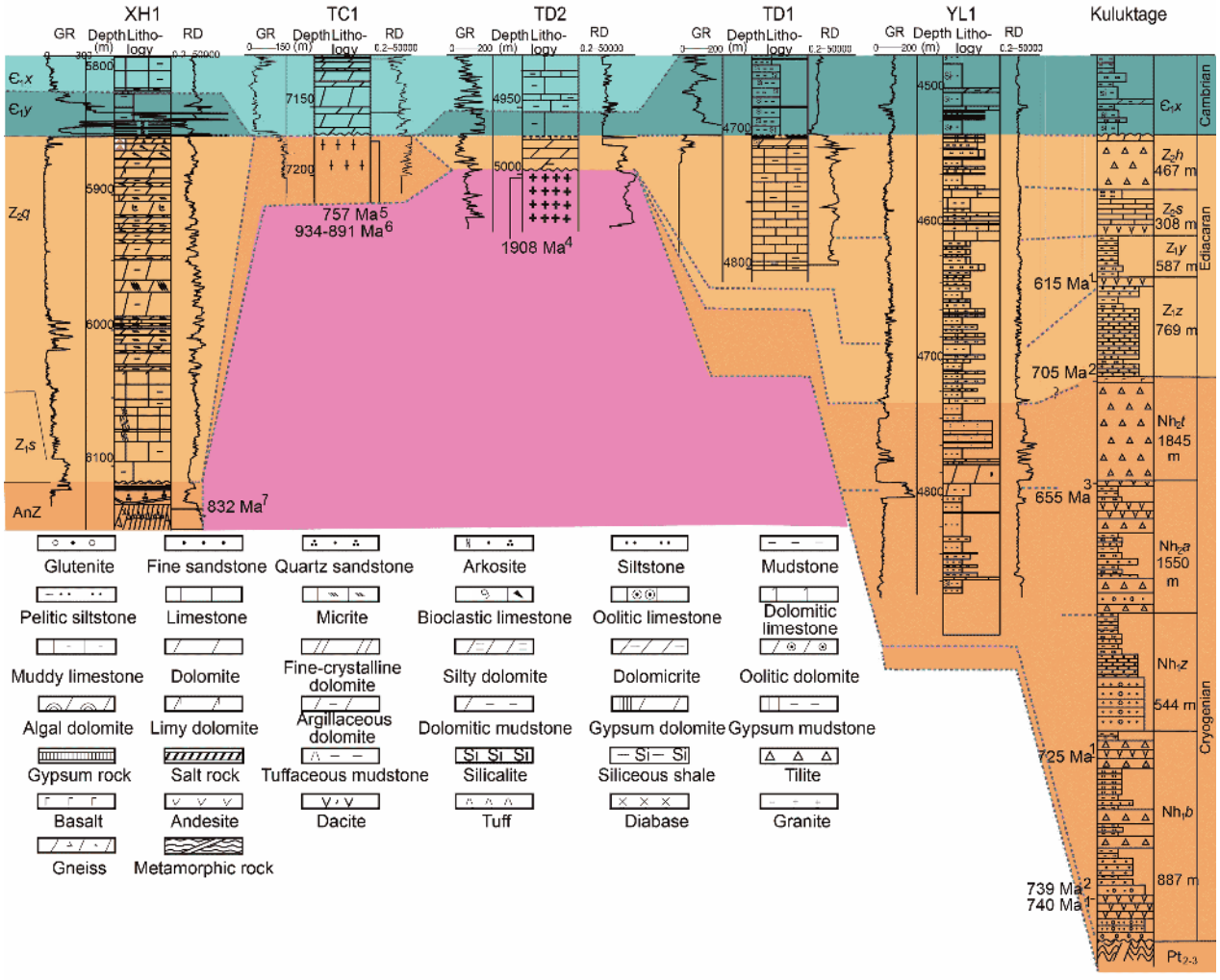

Figure 2 Stratigraphic correlation columns of the eastern and northern parts of the Tarim Basin. References or dating ages: 1, Xu et al. (2009); 2, Gao et al. (2010); 3, He et al. (2014); 4, Wu et al. (2012); 5, Guo et al. (2005); 6, Li Y J et al. (2003); 7, Xu Z Q et al. (2013). The vertical scales of the outcrop and drillholes in this figure are different, and that in Figure 3 is similar. The lithological column in the Kuluktage area are modified from Gao et al. (2010) and Xu et al. (2005, 2009). Strata: Z-Sinian, equivalent to the Ediacaran; Nh-Nanhuaian, equivalent to the Cryogenian. In the basin and the Kepingtage area, Nh_1q-Qiaoenbrak Fm. of Nh_1; Nh_2y-Yuermeinak Fm. of Nh_2; Z_1s-Sugetbrak Fm. of Z_1; Z_2q-Chigebrak Fm. of Z_2; $\in_1y$-Yuertus Fm. of the Lower Cambrain ($\in_1$); $\in_1x$-Xorburak Fm. of the $\in_1$. In the Kuluktage area, Nh_1b-Bayisi Fm. and Nh_1z-Zhaobishan Fm. of the Nh_1, Nh_2a-Altungol Fm. and Nh_2t-Tereeken Fm. of the Nh_2; Z_1z-Zhamoketi Fm., Z_1y-Yukengol Fm. of the Z_1, Z_2s-Shuiquan Fm. and Hankalchough Fm. of the Z_2, $\in_1x$-Xishanburak Fm. of the $\in_1$. In the West Kunlun area, Qb_1s-Sukuluoke Fm., Nh_1y-Yalaguzi Fm. and Nh_1b-Bolong Fm. of the Nh_1; Nh_2k- Keliya Fm. and Nh_2y-Yutang Fm. of the Nh_2; Z_1k-Kuerkake Fm. of the Z_1 and Z_2k-Kezisuhumu Fm. of the Z_2, $\in_1y$-Yuertus Fm., $\in_1x$-Xorburak Fm., $\in_1w$-Wusongor Fm.

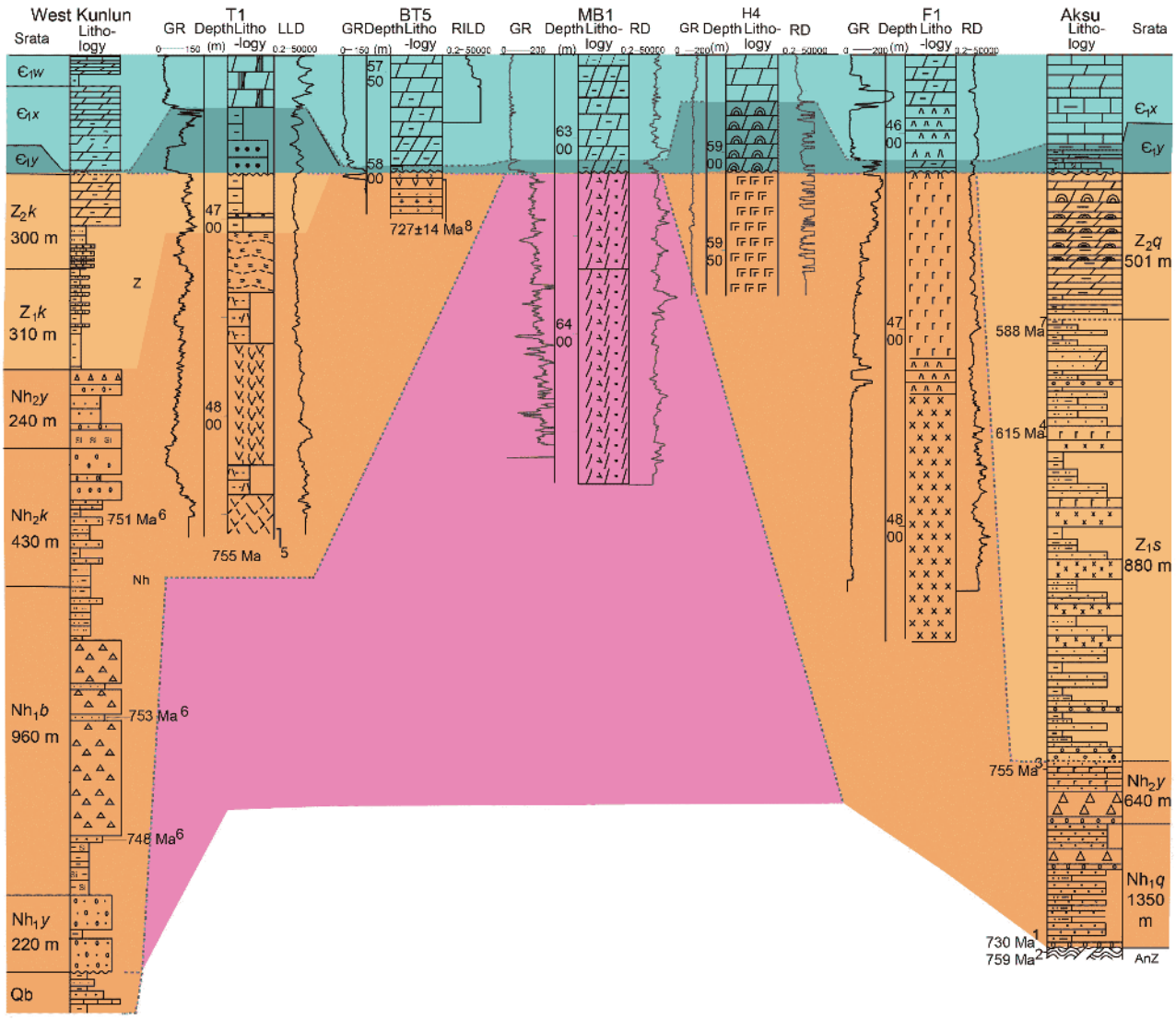

Figure 3 Stratigraphic correlation columns of the western and southern parts of the Tarim Basin. References or dating ages: 1, Zhu et al. (2011); 2 Zhang C L et al. (2012a); 3, Wang et al. (2010); 4, Xu B et al. (2013); 5, Xu Z Q et al. (2013); 6, Zhang et al. (2016); 7, He et al. (2014); 8, this paper. The column of the West Kunlun area is modified from Wang F T et al. (2006), Gao et al. (2013), Zhang et al. (2016); the column of the Aksu area is modified from Zhu et al. (2008), Wang et al. (2010), Xu B et al. (2013).

dolomites (Figure 3). Among them, the Yourmeinak Formation is dominated by magenta tillites, which are similar to the glacial deposits of the Tereeken Formation. in the Kuluktage area (Gao and Zhu 1984). There are also continental tholeiites in the Sugetbrak Formation (Wang et al., 2010). The Aksu Group is composed of glaucophane schists, actinolite schists, epidote-actinolite schists and albite-quartz schists (Xiao et al., 1990; Nakajima et al., 1990; Zheng et al., 2008). These were all derived from volcanic and pyroclastic rocks and developed during the late Paleoproterozoic-early Neoproterozoic (Xiao et al., 1990; Gao et al., 1993; Zheng et al., 2008), while the timing of the metamorphism is in the late Neoproterozoic (760–730 Ma) (Zhu et al., 2011; Zhang et al., 2012a; Yong et al., 2013; Figures 1 and 3).

The first set of un-metamorphosed sedimentary rocks is the Annanba Group of the Neoproterozoic at the northern end of the Altun Mountain in the southeast margin of the Tarim Basin, which is in unconformable contact with the Milan Group It is composed of purplish-red pebbly sandstones on the bottom and transitions upward into thick dolomites and dolomitic limestones on the top (Lu et al., 2008; Zhang et al., 2011). Large oblique bedding and cross-bedding occurred in the purplish pebbly sandstone layers, while thick stromatolite-bearing dolomites occur in the upper dolomite section. The Milan Complex (Li et al., 2001; Lu et al., 2008) is mainly composed of different types of mafic granulites, amphibolites, and TTG granites. It has experienced three phases of thermal events before the Neoproterozoic during 2.8–2.6, 2.45–2.35 and 2.0–1.8 Ga (Che and Sun, 1996; Li et al., 2001; Gehrels et al., 2003b; Lu et al., 2008;

Zhang J X et al., 2011, 2012). Three tectonic thermal events were also shown to have occurred in the Altun area: early Neoproterozoic (900–940 Ma) (Gehrels et al., 2003a; Lu et al., 2006; Wang C et al., 2006), late Neoproterozoic (*ca.* 760Ma) and early Palaeozoic (490–450 Ma) (Zhang J X et al., 2005a, 2007; Luo et al., 2009).

The Silu and Qiakmakelieke groups of the Neoproterozoic are the first set of sedimentary cover in the West Kunlun area on the south margin of the Tarim Basin (Zhang et al., 2016). The Silu Group of the Tonian is composed of the Bochatetage, Sumalan and Sukuluoke formations, and is dominated by clastic rocks and carbonates. The Cryogenian is composed of the Yalaguzi, Bolong, Keliya and Yutang formations (Zong et al., 2010; Zhang et al., 2016; Figure 3), and is characterized by purplish-red conglomerates and glutenites, greyish-green silicalites, purplish-red or greyish-green diamictites and tillites, purplish red sandstones, conglomerates and siliclastics rocks. In the early stage, there were a large number of dyke swarms, bimodal volcanics and evoloved alkaline granites (Zhang et al., 2003, 2016). Two glacial periods of the Bolong Formation and the Yutang Formation of the Qiakmakelieke Group can be compared with the Bayisi Formation and Altungol-Tereeken formations in Kuluktage area. An unconformity separates the Ediacaran and Cryogenian sequences. The Ediacaran is composed of grayish-black mudstones, greyish-green mudstones, and silty mudstones of the Kuerkake Formation, and grey phosphorous sandstones, purple grey dolomites of the Kezisuhumu Formation. The basement in this area composed of the Heluositan Complex of the Paleoproterozoic (Zhang et al., 2007b) and granitic gneisses of the Karakash Group (Hu and Wei, 2006).

Several drillholes in the Tarim Basin are missing of the Cryogenian and Ediacaran strata (Xu Z Q et al., 2013; Wu et al., 2016). The Xorburak Formation of the lower Cambrian is in direct contact with the late Paleoproterozoic basement. Some drillholes revealed the Cryogenian and Ediacaran and can be compared with the Neoproterozoic of the peripheral orogenic belts of the basin (Figures 2 and 3). The Chigebrak Formation (Z_2q) is revealed as the main strata of the Ediacaran in the north-central Tarim basin. It is mainly composed of dolomicrites, silty-finely crystalline dolomites, microorganism-rich, finely crystalline dolomites, stromatolite crystalline dolomites, and clotted dolomites. The lithologies of Well XH1 in the Tabei Uplift and TD1 and TD2 in the Tadong Faulted Uplift correspond to the outcrops in the Aksu area; the Well YL1 in Kongquehe Slope corresponds to the Shuiquan and Hankalchough formations in the Kuluktage area and the Kezisuhumu Formation in the northern margin of the West Kunlun area. Only Well YL1 in the Kongquehe area intersected the Sugetburak Formation of the basin. It is characterized by purplish-red and greyish-green sandstones interbedded with mudstones, and can be compared to the Kuerkake Formation in the northern margin of the West Kunlun orogenic belt and the Yukengol and Zhamoketi formations in Kuluktage area. Unlike in the outcrops, igneous rocks in Well YL1 are seldom developed. The Cryogenian in the basin are mainly composed of clastic rocks, such as maroon coarse sandstones and mottled conglomerates (intersected in Well BT5 and Well S57), as well as igneous rocks such as andesites and dacites (Well T1), basalts (Well BT5) and granites (Well TC1 and Well YD2), which are highly differentiated. Well YL1 intersected the many formations of the Cryogenian; the Tereeken Formation is mainly composed of white, sandy dolomite, argillaceous dolomites, greyish-green quartz sandstones, grey marlites and sandy limestones; the Altungol Formation is mainly composed of greyish-green, blue-grey, and dark grey mudstones interbedded with grey silty mudstones and argillaceous siltstones, which can be compared with those in the Kuluktage area (Figure 2). The tillites were only found in cores of the Tabei Uplift (Well S57) and Bachu Uplift (Well BT5), and are difficult to identify in uncored well sections.

4. Characteristics of the Neoproterozoic rifting depression groups

The Tarim Basin is a multi-period superimposed basin, in which the Neoproterozoic is difficult to identify because of the multiple late-stage tectonic events, the huge-hickness of overlying Phanerozoic sedimentary strata, a vast desert, as well as the poor quality of the deeper reflections of the seismic data. In this study, we mainly used 18 deep drillholes, which were drilled into the Precambrian and distributed throughout the basin, and 27 reprocessed 2D seismic reflection profiles with higher SNRs across the basin, which were reprocessed by the Oil and Gas Investigation Centre of the Chinese Geological Survey (in 2014–2015), as well as many local 2D and 3D seismic reflection profiles which are acquisited and processed by SINOPEC and CNPC in the Tarim Basin. We systematically analysed the Neoproterozoic tectonics of the basin using combined borehole and seismic data, and identified many rifting depression groups of the Cryogenian and Ediacaran (Figure 4).

4.1 Characteristics of the Neoproterozoic Faults

The major Neoproterozoic faults are dominated by normal faults (Figures 4 and 5), and individual faults have strike-slip features. Most of faults cut the basement and have combination patterns of stepped, Y-shaped, grabens, and horsts in profile. The fault displacements are generally 300–800 m, although the largest vertical displacement occurred on the South Yingjisu Fault in the eastern part of the basin, and may exceed 4000 m (AA′ in Figure 5). The dip angles of the faults

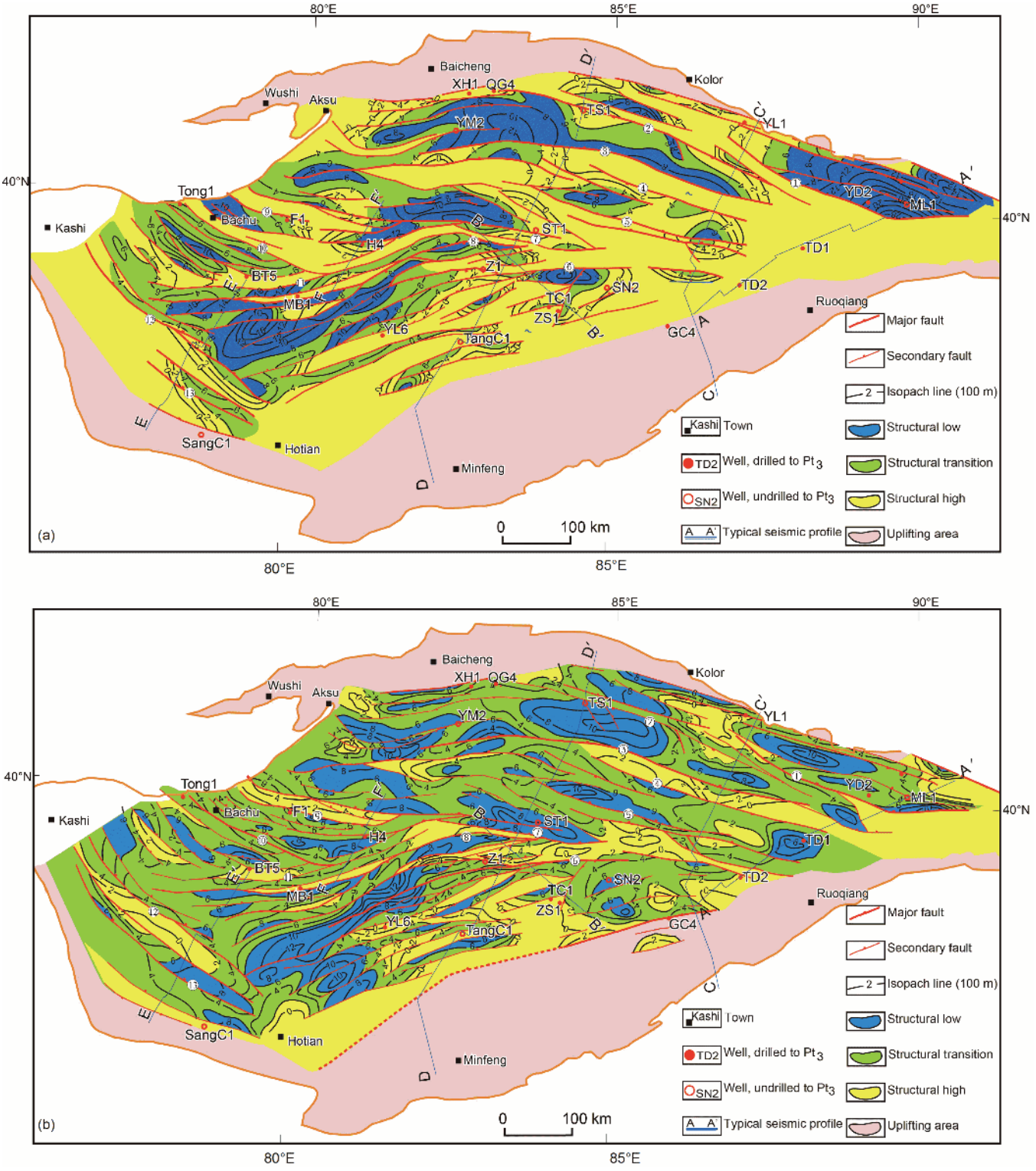

Figure 4 Distribution of the rifting depressions of the Cryogenian and Ediacaran, Tarim Basin. (a) Cryogenian, (b) Ediacaran. Major faults: ① South Yingjisu Fault-SYJS F.; ② South Kongquehe Fault-SKQH F; ③ Yingmaili-Tahe Fault-YML-TH F.; ④ North Manjiaer Fault-NMJE F.; ⑤ South Manjiaer Fault-SMJE F.; ⑥ South Shuntuoguole Fault-SSTGL F.; ⑦ North Shuntuoguole Fault-NSTGL F.; ⑧ West Tazhong Fault-WTZ F.; ⑨ Tumuxiuke Fault–TMXK F.; ⑩ South Haimiluosi Fault SHMLS F.; ⑪ East Maigaiti Fault-EMJE F.; ⑫ North Shache Fault-NSC F.; ⑬ Hotan Fault-HT F.

vary widely from 20°–80° (Figure 5). The strike direction of the faults vary mainly from WNW, ENE, to NE (Figure 4), while the main fault belts extend about 300–400 km along strike, with some only 20–50 km. Moreover, the strike directions of the faults clearly have dominant regional distributions. The WNW-trending faults are mainly in the

northern and central parts of the basin, the ENE-trending faults are in the southern and central parts, while in the southwestern part the faults are again WNW-trending. Many faults are characterized by groups with oblique distributions. Among them, there are 12 major faults that control the development of the major fault depressions. The major faults can be composed of several secondary faults which are distributed in echelon (Figure 4).

The activities of the main Neoproterozoic faults controlled the development of the Cryogenian and Ediacaran, and there activities were clearly different in time and space (Figures 5 to 8). As recognition of the Neoproterozoic fault systems and their particularities are still in the initial stages, and in order to reflect their controls on the fault depressions, regional names are used to name the major faults in this paper (Figure 4). Except for individual reactivated faults that later underwent inversion, such as the Tumuxiuke Fault in the central and western parts of the basin and the South Yingjisu Fault in the eastern part of the basin (Figure 4), which had been normal faults in the Neoproterozoic and turned into thrust faults in the early Palaeozoic (Figure 5a, South Yingjisu Fault), the activities of most other faults weakened and eventually ceased at the end of the Ediacaran or Early Cambrian (Figure 7b, West Tazhong Fault). Also, less faults displayed weak thrusting activities at the end of Ediacaran to Early Cambrian. The main periods of activity and strength of the major faults were different, such as the East Maigaiti Fault and the South Yingjisu Fault during the Cryogenian, while the West Tazhong-North Shuntuoguole Fault, the Yingmaili-Hudson Fault, and the South and North Manjiaer Faults (Figure 4) were mainly active during the late rifting in the Ediacaran.

According to the stratigraphy cut and the depositional control of the Neoproterozoic faults, the major faults were mainly active during the Cryogenian to Ediacaran, and most of them eventually ceased at the end of the Ediacaran, while some displayed weaker activities during the Early Cambrian. Individual faults were reactivated in the Ordovician (He et al., 2011) and Permian with the properties of normal fault (Figures 5 to 8).

4.2 Distribution of Neoproterozoic rifting depressions

The Neoproterozoic faulting activities controlled the development of the rifting depressions in the Tarim Basin, by constraining the structural patterns of the fault depressions (grabens), half-grabens, and horst-grabens (Figure 4, Figures 5 to 8). They also controlled the stratigraphic deposition in the rifting depressions. Rifting depressions mostly formed on the Precambrian metamorphic and crystalline basement, and unconformably underlie the lower Cambrian (Figures 5 to 8). Controlled by the fault systems, three rifting depression groups formed in the northern, central southern, and southwestern parts of the basin, and were distributed in belt shapes.

(1) The northern rifting depression group in the Tarim Basin is distributed in the present Awati-Manjiaer Depression and Tabei Uplift. Controlled by the major faults of the South Yingjisu, South Kongquehe, Yingmaili-Hadexun, South Manjiaer, North Manjiaer and North Shuntuoguole, five major rifting depressions are formed with an almost WNW-trend (Figure 4). The South Yingjisu Fault Depression is recognized as having the maximum subsidence amongst the rifting depressions. It is controlled by the NW-trending, east-dipping, South Yingjisu Fault (Figure 4, and profile AA′ in Figure 5), and is accompanied by many secondary faults. The structural style corresponds to a half-graben with the southwestern margin faulted and northeastern margin overlapped. The thickness of the Neoproterozoic is up to 4100 m, while the area of depression is 3.6×10^4 km^2. In the late Ediacaran, the fault activity weakened, and local segments of the faults were reactivated and inversion occurred with thrusting during the Late Ordovician and Mesozoic. The Yingmaili-Tahe and East Manjiaer Fault Depression was controlled by the Yingmaili-Hadexun Fault and the South Kongquehe Fault (Figures 4 and 7), and represent the largest area of faulted depressions with the total area is 9.0×10^4 km^2. It shows a half grabens structural style with southern margin faulted and the northern margin uplifted, and consists of three subsidence centres (secondary depressions). The Manjarer Fault Depression is controlled by the South Manjarer and North Manjarer Faults and is characterized by asymmetrical double-edged faulting (Figures 4 and 6). The Shunbei Fault Depression is controlled by the North Shuntuoguole Fault (Figures 4 and 7), and presents a half-graben structural style with the southern margin faulted and the northern margin overlapped, while the thickness of the Neoproterozoic is up to 1600 m.

(2) The central-southern rifting depression group is located in the eastern parts of the present Maigaiti Slope and Bachu Uplift, and passes northeastwards through the Tangguzibasi Depression and finally to the central parts of the Tazhong Uplift (Figure 4). The rifting depression group is mainly controlled by a series of NE-trending or ENE-trending normal faults, with the northwestern margin faulted and southeastern margin overlapped, and consists of seven fault depressions of various sizes. The East Maigaiti- East Bachu Fault Depression is located in the southwestern part of the area (Figure 8). It has a large range and intense subsidence, with four secondary subsidence centres. The total area of the depression is 4.5×10^4 km^2, and the thickness of the Neoproterozoic is up to 2200 m. The eastern part of this rifting depression group is controlled by ENE-trending, EW-trending and WNW-trending faults, which form a narrow NE-trending or ENE-trending strip-shaped half graben zones, including the four fault depressions of the West Taz-

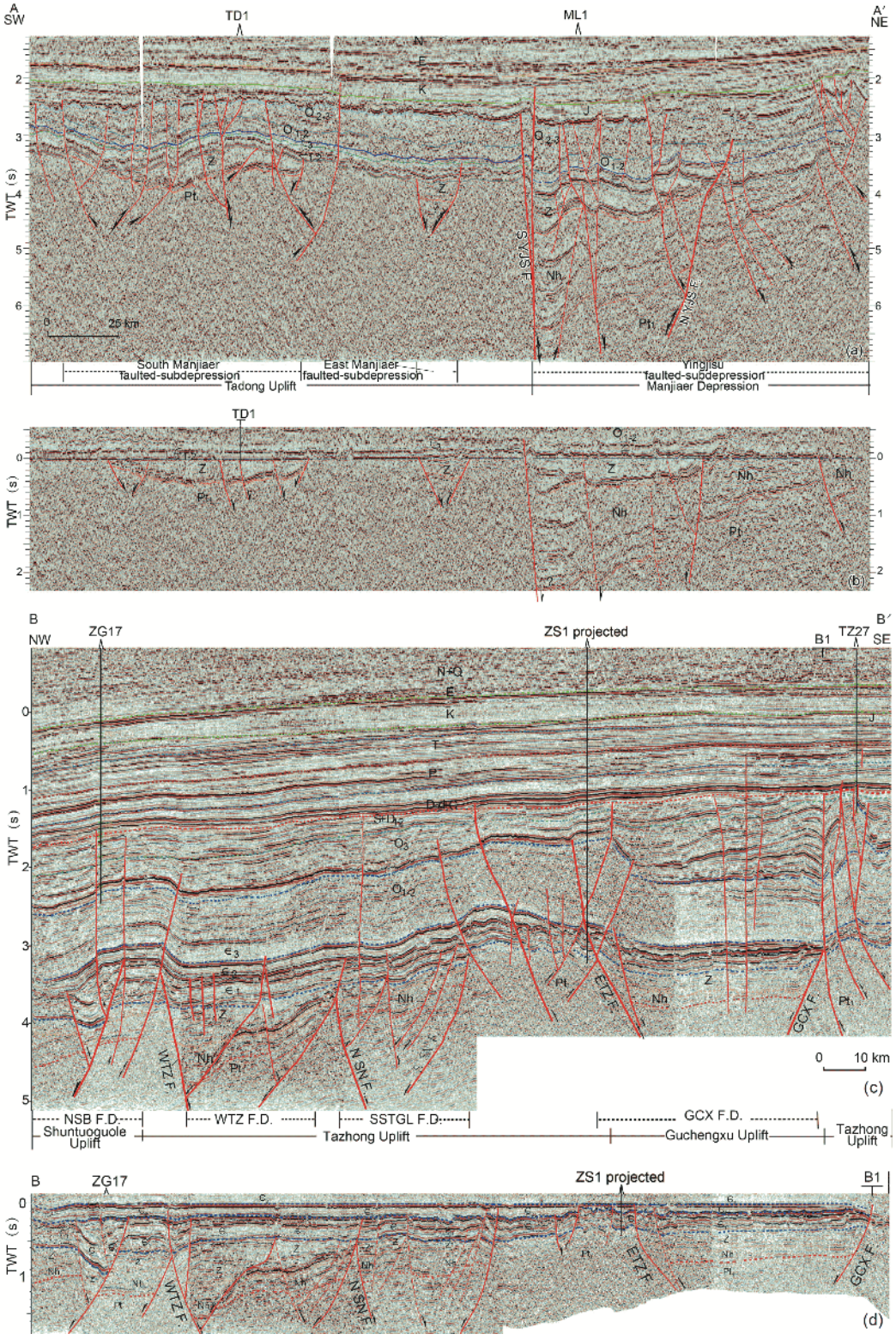

Figure 5 Geological interpretation seismic profiles across the southeastern and central parts of the basin and showing the rifting depressions of the Cryogenian and Ediacaran, Tarim basin. (a) Manjiaer and Yingjisu Fault Depressions; (b) horizon-flattening by the reflection waves at the bottom of the Cambrian for profile A-A′ (a), showing the characteristics of normal faults, and the faults clearly controlling the thicknesses of the Cryogenian and Ediacaran in the hangingwalls; (c) West Tazhong Fault Depression, profile B-B′; (d) horizon-flattening by the reflection waves at the bottom of the upper Cambrian for the profile B-B′. The solid line at the bottoms of profiles shows the structural units of the Phanerozoic in the Tarim Basin, while the dash line shows the Cryogenian and the Ediacaran rifting depressions and their ranges. The locations of the profiles are shown in Figure 4. Fault: ①, SYJS-South Yingjisu; ⑦, SSN-South Shunnan; ⑥, NSN-North Shunnan; ⑧, WTZ-West Tazhong; ETZ-East Tazhong; GCX-Guchengxu. The circled numbers of the faults are marked in Figure 4.

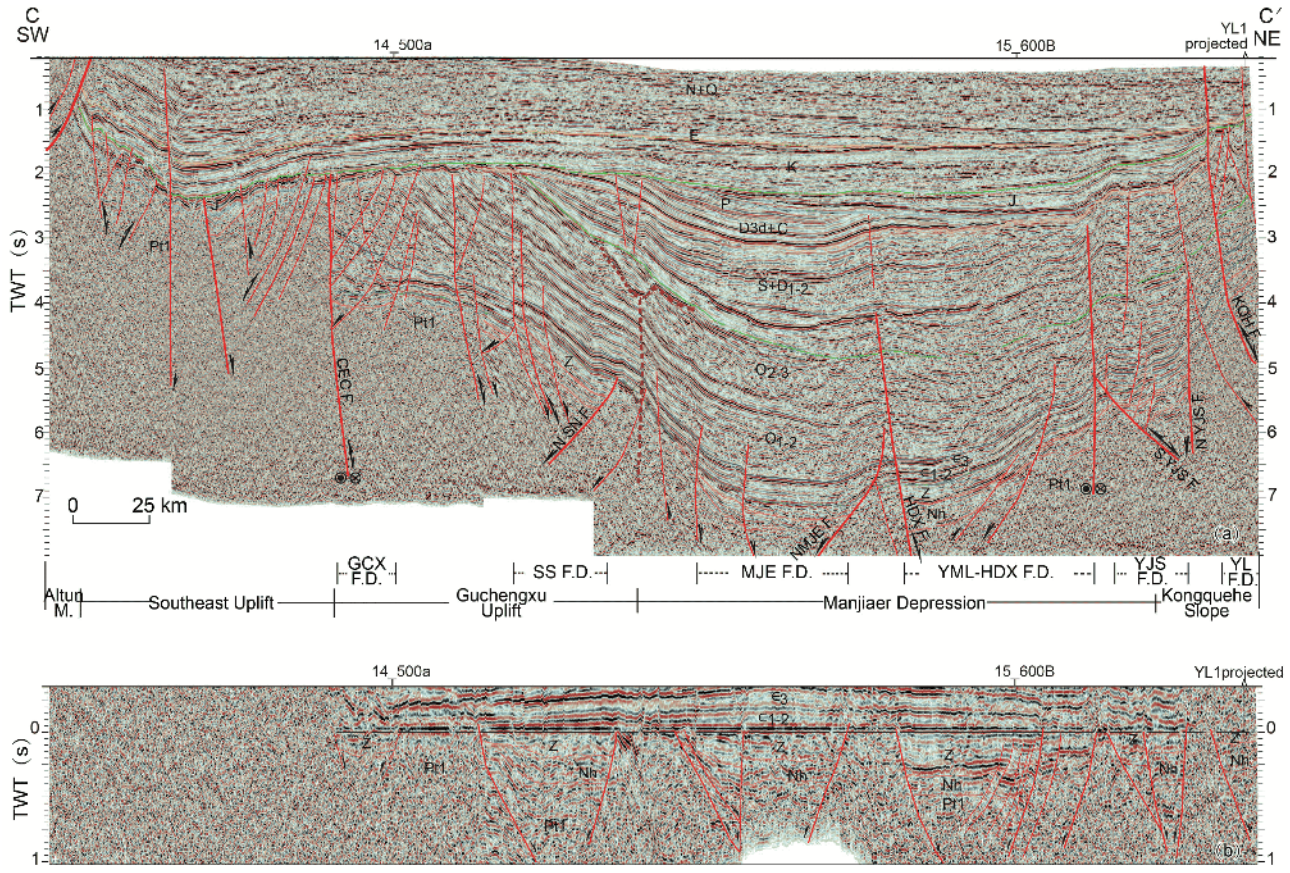

Figure 6 Geological interpretation seismic profile CC′. (a) Across the eastern parts of the basin and showing the rifting depressions of the Cryogenian and Ediacaran; (b) horizon-flattening by the reflection waves at the bottom of the Cambrian for profile CC′. The annotations at the bottom of the profiles are the same as in Figure 5, while the location of the profile is shown in Figure 4. Fault(F.): CEC, Cheercheng; NSN, North Shunnan; NMJE, North Manjiaer; HDX, Hadexun; SYJS, South Yingjisu; NYJS, North Yingjisu; KQH, Kongquehe.

hong, East Tazhong, Guchengxu, and South Shunnan, where the area of individual depressions has a range of about 0.43×10^4–0.63×10^4 km^2. The West Tazhong Fault Depression with nearly an almost EW-trend is controlled by the West Tazhong Fault Zone, forming a half-graben with the northern margin faulted and the southern margin overlapped (B-B′ in Figure 5). The Shunnan Fault Depression is controlled by the South Shunnan Fault and North Shunnan Fault with the WNW-trend and opposing-dipps. It is of the double-edged faulted structural style, and presents two sub-depressions andcontrolled by the NE-trending faults. The East Tazhong and Guchengxu Fault Depressions are controlled by ENE-trending faults, which form half-grabens that are faulted in the northern margin and overlapped on the southern margin.

(3) The southwestern rifting depression group is located in the southwest of the basin, involving the Southwestern Depression Zone and the West Maigaiti Slope of the present-day. The fault depressions mainly show a WNW -trend. The eastern and northern margins are in contact with the central-southern rifting depression group. The Hotan (E-E′ in Figure 8) and the Bashituo Faulted Depressions are both half-grabens that with faulted on the southern margin and overlapped on the northern margin, with thicknesses of the Neoproterozoic up to 1200 m.

According to the distribution of the Neoproterozoic rifting depression groups in different periods (Figures 4 to 6), both the Cryogenian and Ediacaran faults have had relatively strong effects. Most of the faults were active up to the end of Ediacaran and even to the early and mid-Cambrian (Figures 5 to 7). The major faults in different depressions have different intensities of activity during the Cryogenian and Ediacaran, resulting in different sedimentary strata filling in these periods. The Cryogenian strata in the East Maigaiti and Yingjisu Fault Depressions are thicker, while the Ediacaran strata are more developed in the Yingmaili-Tahe Fault Depression. Most of the fault depressions indicate that the subsidence centres were shifted significantly eastward along the faults from the Cryogenian to Ediacaran, and the occurrence of multiple small Ediacaran fault depressions in the Tadong area may be related to this.

The angular unconformity between the Ediacaran and the Cambrian (Figures 5 to 8) is clearly in the uplifted parts of the half-grabens. The Ediacaran is truncated, and the Cambrian is overlapped onto the Cryogenian and Ediacaran or older strata. While the Cryogenian presents a growth strati-

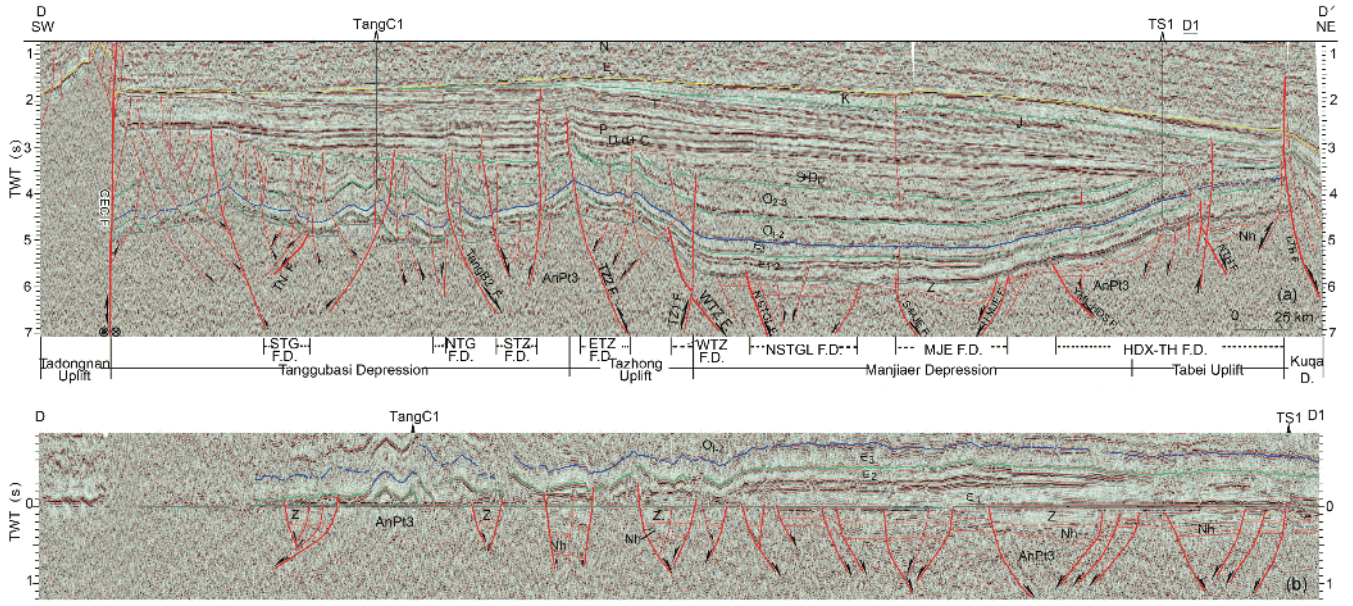

Figure 7 Geological interpretation seismic profile DD′. (a) Across the central parts of the basin with about NS-trending and showing the rifting depressions of the Cryogenian and Ediacaran, Tarim Basin; (b) horizon-flattening on the reflection waves of the bottom of the Cambrian in the part of the profile DD′. The locations of the profiles are shown in Figure 4. Faults(F.): CEC, Cheercheng; TN, Tangnan; TangB2, Tangbei 2; STZ, South Tazhong; TZ2, Tazhong 2; TZ1, Tazhong 1; WTZ, West Tazhong; NSTGL, North Shuntuoguole; SMJE, South Manjiaer; NMJE, North Manjiaer; YML-TH, Yingmaili-Hadexun; NTH, North Tahe; LTB, North Luntai. The annotations at the bottom of the profiles are the same as in Figure 5, while the location of the profile is shown in Figure 4.

graphy controlled by normal faults, they are onlapped or baselapped onto the basement.

5. Discussion on the formation mechanisms of Neoproterozoic rifting depression groups

5.1 Reliability analysis of data

The Neoproterozoic strata formed in the initiation phase of the basin, and were covered by a thick Phanerozoic sedimentary sequences in most of the Tarim Basin. Seismic wave energy is absorbed by the surface desert, igneous rocks of the Permian, gypsum salt rocks of the Cambrian, and so on, as well as the interferenced from many kinds of seismic multiples, make the Neoproterozoic reflection energies weak and the SNRs even lower. This has resulted in a paucity in the understanding of Neoproterozoic geology, such that the Neoproterozoic in the covered area have been very difficult to identify. Based on the stratigraphic correlation framework between the Tarim basin and its peripheral orogens, we have calibrated the Neoproterozoic seismic reflection waves in the seismic reflection profiles using the synthetic seismic records of multiple boreholes, and analysed the characteristics of the reflection wave groups. At the same time, the reflection wave characteristics of the basement and the Cambrian, which were confirmed by wells, have been as auxiliary marks (Figure 9a), and constrained the effective reflection waves of the Neoproterozoic between them. The sedimentary strata and the fault structures of the Neoproterozoic have been systematically identified and interpreted. In undrilled areas, it is mainly based on interpretation scheme networks from throughout the basin, which are constructed from key seismic profiles controlled by the wells. The interpretations have also been combined with the local velocity analyses, seismic multiples identified and eliminated, and the effective reflection waves under the Cambrian identified, such that the Neoproterozoic effective reflection waves have been confirmed (Figure 9b).

The discrimination of the Cryogenian and Ediacaran has been mainly based on the strata developed in outcrops, drilling and logging data, as well as synthetic seismic records. Their reflected wave groups have been determined and further divided the tectonic layers. Many deep wells are still needed to control the precise divisions and compositions of layers.

5.2 Rifting depression groups and aeromagnetic anomalies

The large ΔTa high aeromagnetic anomaly zone with an EW-trend in the central part of Tarim Basin divides the aeromagnetic anomaly record into two regions (Figure 10a). The northern part is a EW-oriented region with a gentle negative magnetic anomaly, and the southern part is a NE-trending alternating positive and negative magnetic anomaly zone, while the southeast part is an area of sharp and frequent variation (Yuan, 1996). There have been many different interpretations on this phenomenon, especially in terms of

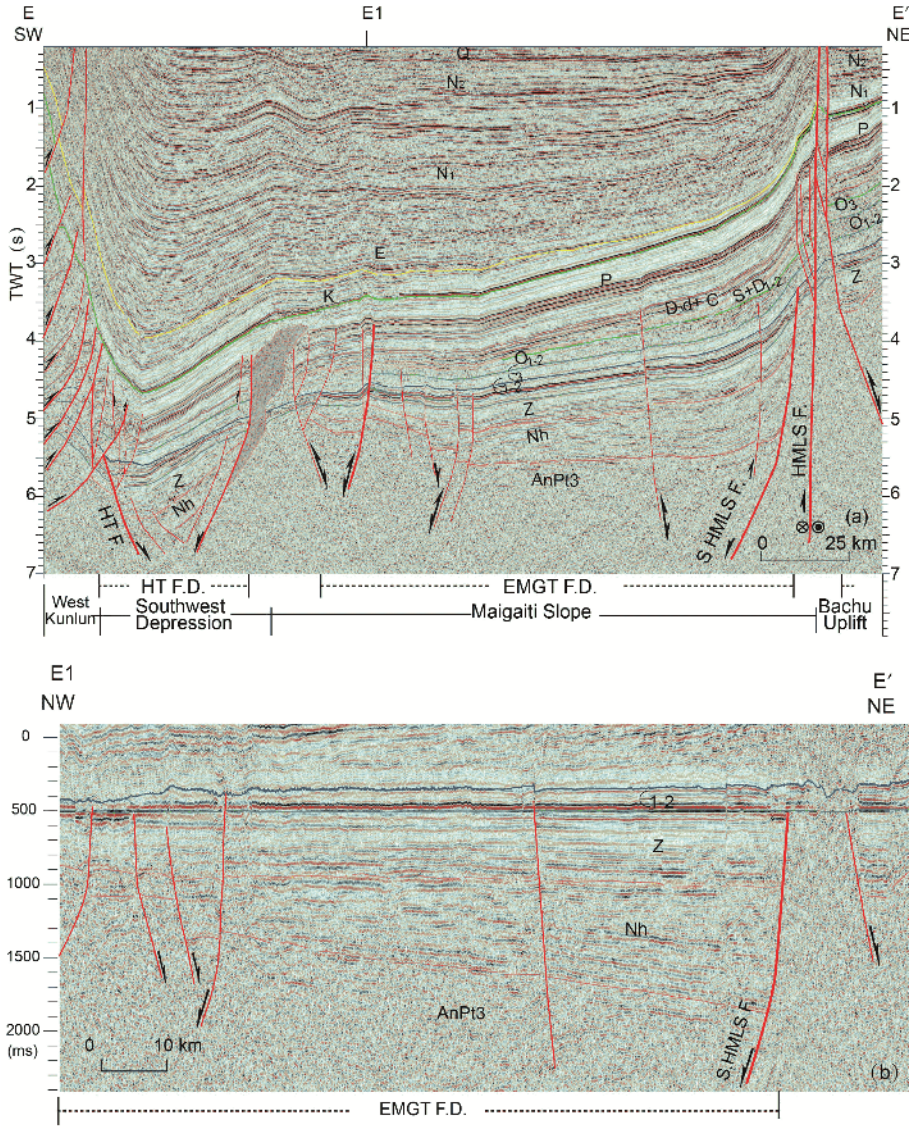

Figure 8 The geological interpretation of seismic profile EE′. (a) Across the Bachu Uplift to the front of the West Kunlun Orogenic Belt with a roughly NS-trend, and showing the rifting depressions of the Cryogenian and Ediacaran; (b) horizon-flattening by the reflection waves at the bottom of the Cambrian in part of the profile EE′. The location of the profile is shown in Figure 4. Fault (F.): HT-Hotan; SHMLS-South Haimiluosi; HMLS-Haimiluosi. The purple-red filled area indicates an igneous body.

understanding the prominent positive aeromagnetic anomaly in the central part and the NE-trending alternating anomalies in the southern part of the basin. These interpretations include: pre-Sinian rifts (Wang et al., 1994); reflections of the basement lithofacies and major deep faults (Xu, 1997); suture of the Jinning Period (Jia, 1997; Guo et al., 2001; Wu et al., 2006), Neoproterozoic rifts and Ordovician igneous rocks (He et al., 2011); and Permian rift and crystalline basement (Yang et al., 2012).

Basic rocks in the Cryogenian or Ediacaran occur in the outcrops in the peripheral orogens of the Tarim Basin, and have strong magnetic properties. For example, the mean magnetic susceptibilities of three layer diabases of the Sugetbrake Formation in the lower Ediacaran, which are located in the Aksu and Urshi areas of the northwest margin of the basin, are 3893.6×10^{-5} SI, 4571.8×10^{-5} SI and 4483.9×10^{-5} SI, respectively (Yang et al., 2012). The peridotites and gabbros of the Proterozoic in the Hongliugou of Altun Mountain at the southeast margin of the basin have maximum magnetic susceptibilities of 23509.8×10^{-5} SI, and an average magnetic susceptibility of 1032.4×10^{-5} SI, which indicate that both the basic and ultrabasic rocks can cause strong magnetic anomalies. In this study, the magnetic properties of cores from several principal exploration wells

1) He B Z, Cui J W, Cai Z H, Li G W, Ma X X, Chen W W, Yu Z Y. 2016. The final report of science research projects 'The structural evolution of the Bachu-Tazhong Uplifts and its implication on the hydrocarbon accumulations'. Northwestern Petroleum Subsidiary of SINOPEC.

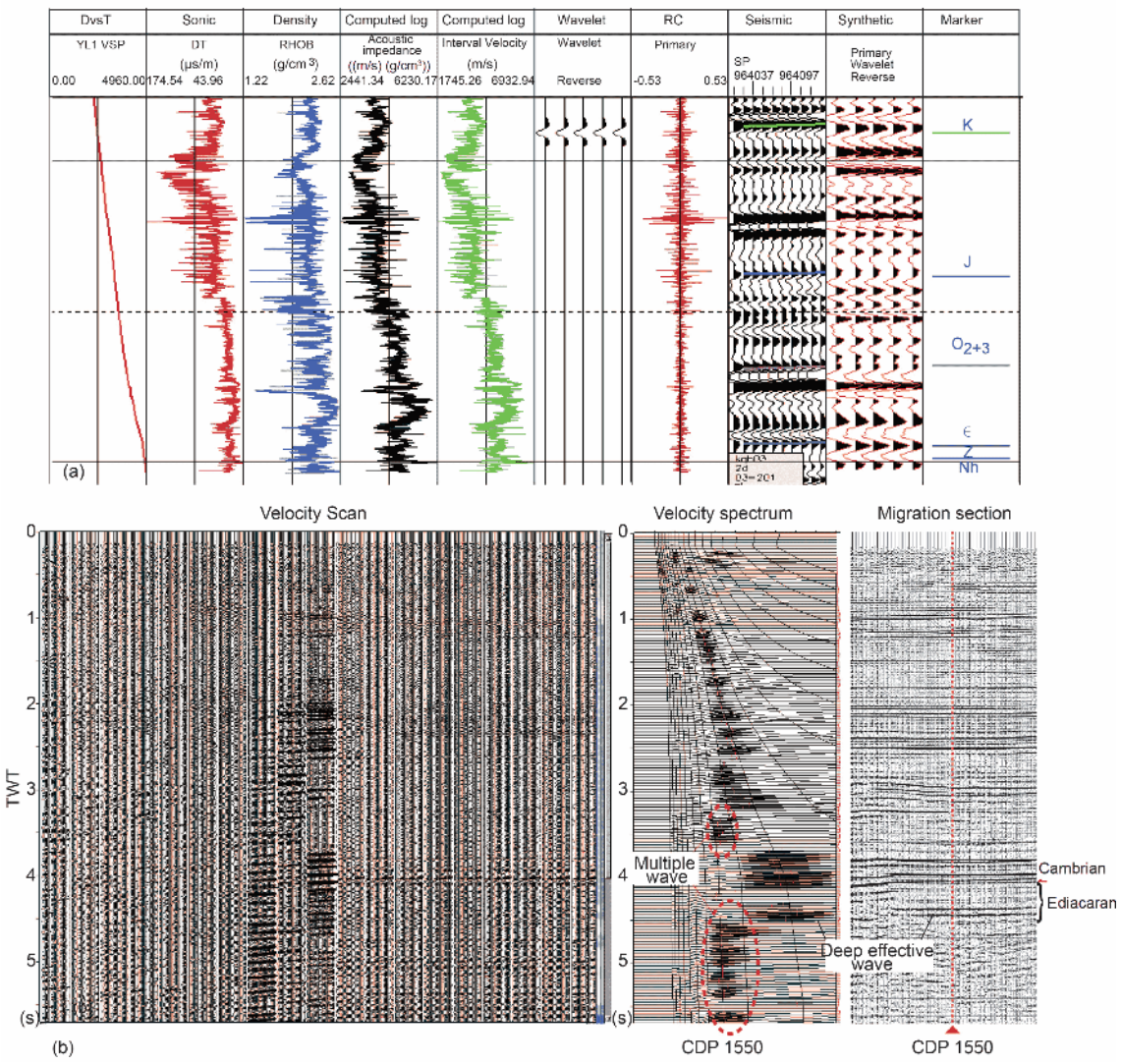

Figure 9 The recognized effective reflection waves of the Neoproterozoic by synthetic seismic records and velocity analyses. (a) Synthetic seismic record of Well YL1; (b) local velocity analyses of the Bachu area. Modified from the Northwestern Petroleum Subsidiary of SINOPEC, 2015.

are analysed (Table 1), and combined with previous research results (Yan et al., 2014) demonstrate that the basic and ultrabasic igneous rocks have higher magnetic susceptibilities, whereas the acid igneous rocks, low-grade metamorphic rocks, and sedimentary rocks have lower magnetic susceptibilities. The lithologies and magnetic susceptibilities of the Wells TZ33, YD2, and Well F1 are quite different (Table 1; Figure 10a).

The fault systems of the Neoproterozoic identified in this study are certainly coordination to the variation zones, mutation zones and gradient belts of the ΔTa aeromagnetic anomalies (Figure 10a). The main parts of the rifting depressions are located in relatively lower aeromagnetic anomalies and negative anomaly areas that reflect the weaker magnetism in these areas. These may be related to sedimentary rocks with weak magnetic properties, while the tectonic transition zones between the southern and northern rifting depression groups are located in the positive aeromagnetic anomaly zone in the centre of the basin. Combined with previous research results, there are five magnetic layers in the Tarim Basin, including: (1) crystalline rocks of the Presinian; (2) basic and ultrabasic rocks of the Sinian; (3) basic and ultrabasic rocks of the Ordovician; (4) basalts of the Permian; and (5) sandstones of the Neogene, all of which have stronger magnetic properties. However, the fault systems of the Phanerozoic in the Tarim Basin are weakly correlated with the gradient belts of the aeromagnetic anomaly (Figure 10b). Therefore, we infer that the aeromagnetic anomaly is a composite effect of the basement properties of the basin, the initial rifts (Cryogenian-Ediacaran) and the late multi-stage magmatic activities (Late Ordovician, Permian, and Neogene). The record of the rifting depressions during the Cryogenian and Ediacaran are contained in the aeromagnetic anomalies. The fault systems are

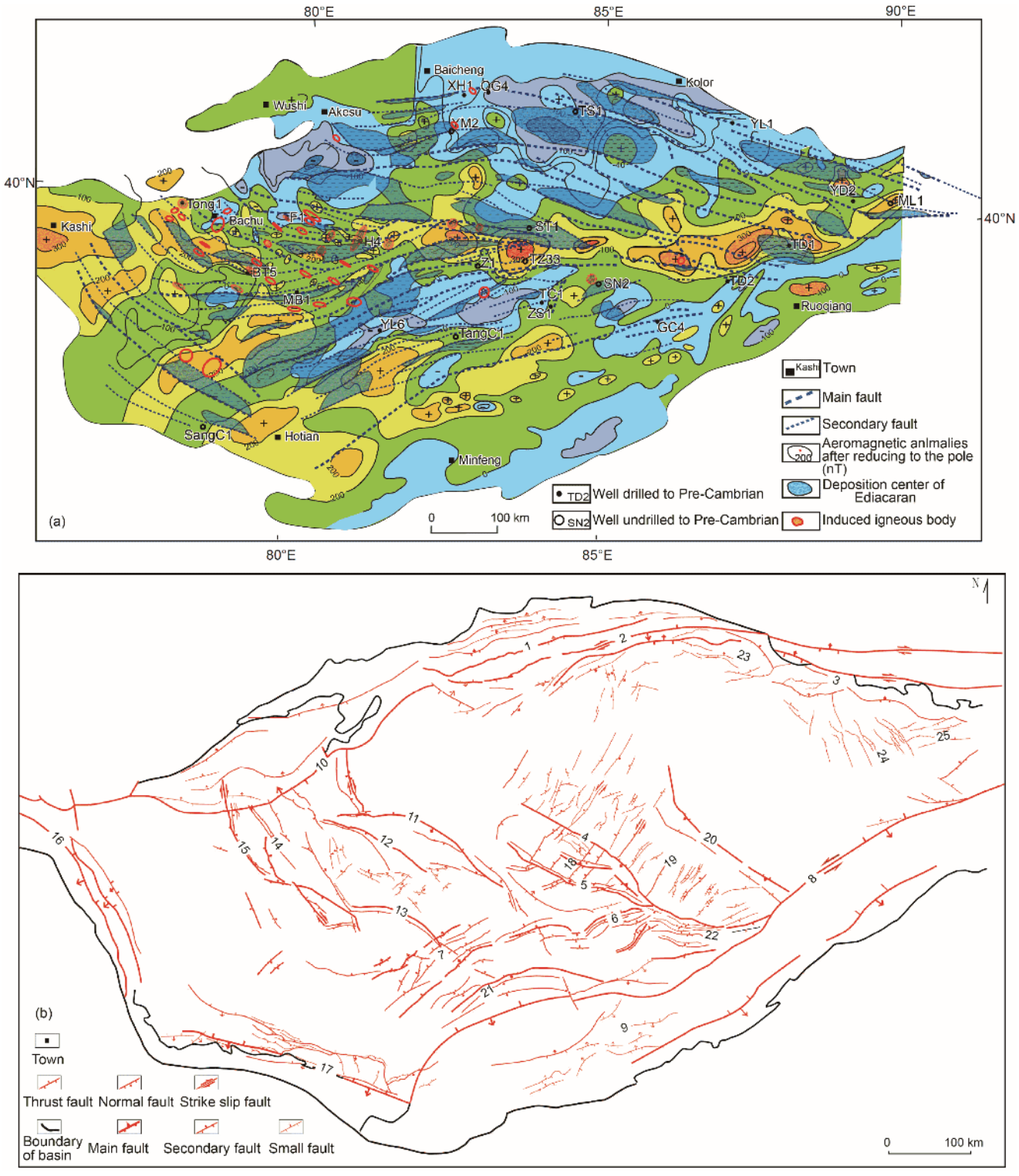

Figure 10 Aeromagnetic anomalies after reduction to the pole, and the rifting depressions during the Ediacaran in the Tarim Basin; (a) Aeromagnetic anomalies map (redrawn from Yuan (1996); and Li Y J et al. (2008)); and (b) fault systems of the Phanerozoic (modified from Tang and Jia (2007); He (2009); Yang et al. (2009); Ren et al. (2011); Huang (2014); Jiao (2017); He et al. (2016)[1]). Fault belts: 1, Kuche; 2, Shaya-Luntai; 3, Kongquehe revier; 4, Tazhong I; 5, Tazhong II; 6, Tazhong III-Tangbei; 7, Madong-Yubei; 9, Mingfeng-Qiemo; 10, Keping; 11, Tumuxiuke; 12, Kalashayi; 13, Mazhatage; 14, Haimiluosi; 15, Selibuya; 16, Kashi; 17, Hotan; 18, Tazhong NE-trending; 19, SHuntuo NE-Trending; 20, Tazhong paltform margin; 21, South Tangguzibasi; 22, Tanggusibasi-Guchengxu; 23, Caohu; 24, Yingjisu NW-trending; 25, Yingjisu EW-trending.

coordinated with variation zones in the magnetic anomaly, especially the high magnetic anomalies that are superimposed on the main faults (Figure 10a), and may reflect the existence of magmatic activity and basic and ultrabasic rocks

Table 1 Magnetization rates of drill cores from the Tarim basin[a)]

Sample	Depth (m)	Lithology	Strata	Mass (g)	Magnetic susceptibility (SI)	Retentivity	Mass Susceptibility (SI/g)	Mass Remanence intensity
F1-2	4750	gabbros	Pt_3	31.23	2.25×10^{-2}	5.45×10^{-1}	7.19×10^{-4}	1.75×10^{-2}
F1-3	4665	diabases	Pt_3	31.02	1.92×10^{-2}	4.62×10^{-1}	6.18×10^{-4}	1.49×10^{-2}
YD2-2	4930	granodoirites	Pt_3	28.2	9.37×10^{-5}	5.46×10^{-3}	3.32×10^{-6}	1.94×10^{-4}
TD1-4	2890	marlites	$\in$	28.11	2.91×10^{-4}	6.68×10^{-4}	1.04×10^{-5}	2.38×10^{-5}
T1-1	2260	diabases	O	7.22	4.22×10^{-3}	2.28×10^{-1}	5.84×10^{-4}	3.16×10^{-2}
T1-2	2265	diabases	O	7.31	5.32×10^{-3}	1.55×10^{-1}	7.27×10^{-4}	2.12×10^{-2}
TZ33	5958	basalts	O	32.35	1.30×10^{-1}	2.17×10^{0}	4.02×10^{-3}	6.71×10^{-2}

a) The tests of the natural remanent magnetic intensity were carried out on the American vertical 2G-755R superconducting magnetometer in the Paleomagnetic Laboratory of the Institute of Geomechanics, Chinese Academy Geological Sciences. The magnetic susceptibilities of the samples were carried out on the KLY-4 susceptibility meter of the AGICO Company, Czechoslovakia, and the natural residual magnetic intensity and the magnetic susceptibility of the unit mass (g) were obtained

(red circles in Figure 10, details will be shown in another paper).

While the sedimentary rocks and small amounts of igneous rocks in the Neoproterozoic occur in the deep wells and outcrops in the eastern and northern parts of the basin, in contrast, basic rocks and intermediate-acid igneous rocks occur in the southwestern of the basin. Integrating the aeromagnetic anomalies and seismic stratigraphic characteristics, the relatively shallow burial depths of the Neoproterozoic rifting depressions in the south and southwest of the basin, and the stronger magnetic anomaly source (5–10 km and 10–15 km depth) in this area (Yang et al., 2012), suggests that igneous rocks of the Neoproterozoic should be more developed in the southern parts than the northern parts of the basin.

5.3 Paleo-stress fields for the rifting depressions formation

During the Cryogenian, the faults of the rifting depression groups in the central and northern parts of Tarim Basin were WNW-trending (average strike direction in 120°–300°), the subsidence centres of the fault depressions were located in the footwalls of the faults and had oblique dextral movement in places. The faults of the central and southern rifting depression groups were NE or ENE trending (average strike directions in 72°–252°) (Figures 4 and 11). During the Ediacaran, the main faults inherited activities, while the strike directions of the faults in the northern rifting depression group were still WNW-trending (average strike direction in 113°–293°), ENE-trending in the central-southern rifting depression groups (average strike direction in 70°–250°), and WNW-trending (average strike direction in 117°–297°) in the south-western rifting depression groups. The differences in the faults between the Cryogenian and Ediacaran are obvious, with the ENE-trending faults becoming more active than the WNW-trending faults. The depocentres migrated eastward along the main faults during the Ediacaran. These types of structural styles illustrate the different structural stress fields that existed in the different units of the Tarim Basin during the Cryogenian to Ediacaran. There was extension with NNW-SSE and NNE-SSW directions in the southern and northern areas, respectively, and this was accompanied by a clockwise torsion. The late extensional actions moved eastward, and the three combined actions formed the structural architecture of the Neoproterozoic in the Tarim Basin.

5.4 Tectonic background and dynamic modelling

The assembly and break-up of the supercontinent affected the formation and evolution of the cratons of the world. The initial development of the Tarim Craton was also closely related to them. The supercontinent Columbia formed during 2.0–1.8 Ga (Rogers and Santosh, 2002; Zhao et al., 2002, 2004, 2012; Zhai and Santosh, 2011), and broke up at about 1.6–1.3 Ga. The break-up event led to the separation of some cratonic blocks from the supercontinent (Zhao et al., 2004; Li Z X et al., 2003, 2008). Between 1.1 Ga and 0.9 Ga, or a little later, a large number of microcontinental blocks converged again with Laurentia to form the Supercontinent Rodinia, which contains almost all of the Precambrian cratons at present, including among them the Tarim Craton. The Supercontinent Rodinia experienced marginal accretion, sustained continental rifting and multiple stages of break-up, and finally complete break-up at 580 Ma (Li Z X et al., 2008, 2013). During this stage, mafic magmatism occurred at three age intervals of 830–790, 780–755, and 745–725 Ma (Li Z X et al., 2003, 2008; Zhu et al., 2011; Wang et al., 2014), mainly related to mantle plumes, the break-up of Rodinia, and the opening of the Proto-Tethys Ocean (Li et al., 1999; Zhu et al., 2011, 2017; Zhang C L et al., 2012a, 2016; Li et al., 2018). These were also accompanied by 3–4 major glacial events (Xu et al., 2009; Gao et al., 2010, 2013; Li et al., 2013).

The Neoproterozoic outcrops in the southern and northern

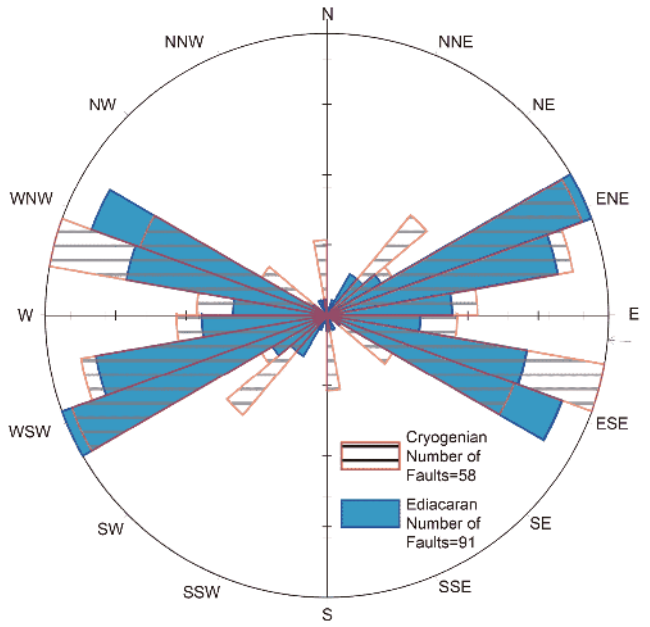

Figure 11 Rose diagram of the strikes of the main faults during the Cryogenian and Ediacaran (relative to the present-day position of the Tarim Block).

margins of the Tarim Basin reveal different Precambrian tectonic events. In the Kolor-Kuluktage area of the northern margin of the Tarim Basin, the high-grade metamorphic age is 830–790 Ma (He Z Y et al., 2012; Ge et al., 2012, 2013) and reflects an accretionary orogenic environment rather than a continental break-up environment in the early and middle Neoproterozoic (Zhu et al., 2017). Basalts (740 Ma), dacites, and rhyolites formed bimodal volcanic rocks at the base of the Bayisi Formation (Xu et al., 2005, 2008), and basalts occurred above tillites at the top of the Bayisi Formation in the Daqixianggou (732 Ma; Xu et al., 2008), whereas volcanic rocks intercalated with clastic rocks at the top of the Altungol Formation (655 Ma; He et al., 2014), pillow basalts occurred in the Tereeken Formation (705 Ma; Gao et al., 2010), basalts and neutral volcanic rocks occurred in the Zhamoketi Formation (614 Ma; Xu et al., 2008), as well as tuffs (616 Ma; He et al., 2014). In addition, a large number of basic dike swarms (634 Ma, Zhu et al., 2011) occurred in the Kolor, and the typical peraluminous granites were found in the core of the Tugelming anticline in the eastern Kuqa Depression (626–643 Ma; He D F et al., 2011). Four sets of globally comparable tillites were developed in the 6000 m thickness of sedimentary record in the rift basin in the Kuluktage area (Xu et al., 2005, 2009; Gao et al., 2010, 2013; Figure 2). The magmatism and sedimentary filling indicate that the northern margin of the Tarim Basin during the middle to late Neoproterozoic (740–615 Ma) was located in a continental rift and intraplate extensional environment.

In the Aksu area of the northwestern margin of the basin, two sets of basalts occurred in the sandy conglomerate layers at the base of the Neoproterozoic (belonged to Sugetbrak Formation is controversial) in an outcrop at Xiaoerbrak. The basalts belonged to the continental tholeiite series, and were derived from an enriched mantle source and suffered variable crustal contamination. The age of the basalts is 755 Ma (Wang et al., 2010). In the northwest of the Sugetbrak area, a basalt (614–615 Ma) occurred in sandstone layers of the Sugetbrak Formation, and formed in an intracontinental rifting environment with 7–12% partial melting. This is different from the large-volume tholeiite (Xu B et al., 2013) representing the waning stage of plume volcanism during a long-lasting continental break-up. The sedimentary records also reflect changes from a continental rift to a passive continental margin sedimentary setting. The thickness of the Neoproterozoic reached up 3300 m (Figure 3). Therefore, the northwestern margin of the basin during the middle to late Neoproterozoic (755–614 Ma) experienced continental rifting environment, in which magmatism weakened later. It is noteworthy that the crystallization age of basalts intruded into fine sandstones of the Sugetbrak Formation (should be the Qiaoenbrak Formation) in the southwest of the Sugetbrak area is 783±2.3 Ma. They were derived from magma originated from partial melting of garnet-spinel peridotite (Zhang Z C et al., 2012), which is related to mantle plume activities and the break-up of the Supercontinent Rodinia.

In the northern Altun Muntain of the southeastern margin of the basin, an ophiolite belt developed in the Hongliugou-Lapiquan area, and gabbros in the Obo area yielded an age of 829±60 Ma from Sm-Nd isotopic dating (Guo, 2000). An early Paleozoic continental subductive ultra-high pressure (UHP), metamorphic belt occurred at the northern margin of theQaidam and southern Altun areas, and the protolith of the eclogite was Neoproterozoic (850–750 Ma) and formed in a continental rifting environment. The surrounding rocks are mainly composed of early Neoproterozoic granite and middle Neoproterozoic or older sedimentary rocks (Zhang et al., 2005; Liu et al., 2012; Song et al., 2010; Zhang et al., 2011, 2015; Wang et al., 2013). Thus, the Neoproterozoic orogenism in the Altun area occurred earlier than that in the Kuluktage and Aksu areas, while the extensional continental rifting environment also occurred earlier (850–750 Ma).

In the west Kunlun Mountain of the southeastern margin of the basin, basic dikes of the Neoproterozoic at Xuxugou emplaced ca. 820–800 Ma, while basalts of the Silu Group yielded ages of 740 Ma. These can be compared to the Bayisi Formation, in that the magma was derived from intraplate transitional mantle or enriched mantle sources, formed in the intraplate extensional environment, and developed in a passive continental margin rifting basin with carbonate-clastic-tillite sequences (Zhang et al., 2007b, 2016). The residual thickness of the Neoproterozoic in the southwestern margin can reach 3300 m (Figure 3). Therefore, the continental rifting and intraplate extension of the Neoproterozoic in the West Kunlun Mountain was similar to that in the Altun area,

but were earlier than the northern margin of the basin.

Several deep drillholes, which were mainly distributed in the uplifts and slopes of the Tarim Basin, intersected the Neoproterozoic. The I-type granite in Well TC1 (Li et al., 2005) was derived from crust-mantle mixed sources, and yielded a zircon SHRIMP age of 757.4±6.2 Ma (Wu et al., 2009). This reveals formation in a tectonic active zone or a intraplate extensional environment (Li et al., 2005; Ge et al., 2012). A sequence of andesites (755 Ma, Xu Z Q et al., 2013), rhyolites, and reddish-brown sandstones occurred in Well T1 at the western end of the Central Uplift Belt. Red-brown conglomerates and basalts (727 Ma; this paper) were intersected by Well BT5, and granites with age of 722 Ma (Xu Z Q et al., 2013) were found in Well YD2 at the eastern end of the basin. Thick-bedded dolomites of carbonate platform facies in the late Ediacaran were intersected by the Well XH1, TD1, and TD2 in the central, northern part and eastern part of the basin. The assemblages of the Neoproterozoic clastic, carbonate, and ignous rocks in Well YL1 represent magmatic activities and sedimentary strata in an extensional environment. The maximum residual thickness of the Neoproterozoic in South Yingjisu rifting depression was about 4100 m according to the interpretation of the seismic data (Figure 4).

Therefore, the Neoproterozoic rifting depressions were the initiation of sedimentary basins in the Tarim Craton, which were controlled by extensional faults with a zonal distribution (Figure 4) and were filled by vast thicknesses of various sediments deposited in terrestrial and marine facies. The multiple periods of volcanic activities, such as mafic-dike swarms, bimodal volcanic rocks, and A-type granites, can be divided into four phases, including 830–800, 780–760, 750–725, and 650–615 Ma (Xu B et al., 2005, 2009, 2013; Zhang et al., 2003, 2012b; Zhu et al., 2008; Zhang et al., 2009, 2016; Xu Z Q et al., 2013; Zhu et al., 2017; this paper). Based on the activities of synsedimentary faults, tectonic thermal events and filling sediments, the rifting depression groups were formed in an extensional environment within a continental intra-plate setting, and the main growth periods of these were 0.8–0.61 Ga. The volcanic activities were abundant and stronger in the western parts of the basin (Figure 10). They also show that rifting during the Neoproterozoic in the Tarim Craton was a long-term, continuous and pulsating process, which has characteristics that are both quasi-coincident with the Supercontinent Rodinia and unique in themselves. The rifting depression groups occurred as a synchronised product of the Rodinia supermantle plume in the Neoproterozoic, intra-plate rifting, and glacial actions, and are similar to those in Australia and the Yangtze Craton (Powell et al., 1994; Li Z X et al., 2008; Zhu et al., 2017). Although the complete separation time of the Tarim Block and its peripheral microcontinental blocks remain uncertain (Safonova et al., 2008; Safonova and Santosh, 2014; Wang et al., 2014; Zhang J X et al., 2015; Zhang et al., 2016; Zhu et al., 2017), the development of rifting depression groups in the Tarim Basin is also related to the initial splitting of the West Kunlun-Altun Ocean and the Paleo-Asian Ocean, and the occurrences of oceanic crust (Figure 12). The successive opening of the West Kunlun-Altun Ocean at the southern margin and the Paleo-Asian Ocean at the northern margin of the Tarim Basin may be the cause of the rifting and clockwise twisting in the basin.

The initiation of the Tarim cratonic basin is similar to other craton basins around the world in terms of their geodynamic background. Most of basins originated in certain extensional environments at the plate-scale (Allen and Armitage, 2012; Guiraud et al., 2005; Persaud et al., 2017). In the Tarim Basin, the depths to the Moho and Conrad discontinuities are 37–44 and 15–38 km, respectively. These have been significantly deepened to 42–54 and 32–44 km at the mountain front zones of the Tianshan, West Kunlun and Altun Mountain belts. This indicates that the upper mantle has been uplifted and the crust thickness has been relatively thinner in the Tarim Basin. Based on the gravity inversion and magnetic data, the thickness of the middle-upper crust varies greatly, while the thickness of the lower crust is relatively stable and generally 16–22 km (Yin et al., 1998). According to the interpretation of the seismic data, the thickness of the

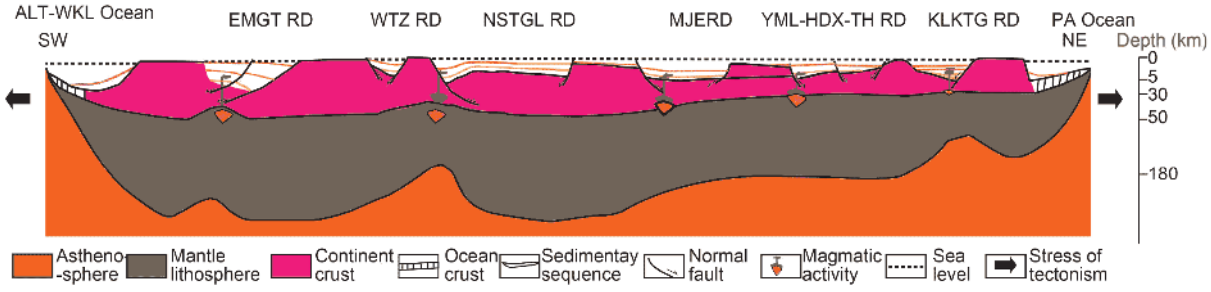

Figure 12 Schematic diagram of the dynamic model of rifting depression formation during the Cryogenian to the Late Ediacaran in the Tarim Basin (redrawn from Yin et al., 1998; Liu et al., 2005; Ingersoll, 2012). In order to highlight the structural architecture of the Neoproterozoic, the vertical dimensions of the profile are not to scale. RD, Rifting Depression; ALT-WKL Ocean, Altun-West Kunlun Ocean; EMGT, East Maigaiti; WTZ, West Tazhong; NSTGL, North Shuntuoguole; MJE, Manjiaer; YML-HDX-TH, Yingmaili-Hadexun-Tahe; KLKTG, Kuluktage; PA Ocean, Plaeo Asian Ocean.

upper to middle crust in the Tarim Basin is 4–14 km (He et al., 2016), while the maximum thickness of the Neoproterozoic is about 4.1 km; and combined the previous research results of the crust-upper mantle structure (Yin et al., 1998; Zhao et al., 2008; Hou and Yang, 2011),the Neoproterozoic rifting and fault depressions in the Tarim Basin were formed in the stress fields generated by mantle uplifting and extension spanning multiple periods.This was accompanied by the generation of igneous rocks due to partial melting, especially in the south. However, the deep driving mechanism of the lower crust and mantle and the dynamic model still need to be further investigated and discussed.

6. Conclusion

(1) About 20 rifting depressions developed in the Tarim Basin during the Cryogenian and Ediacaran. They overlie Precambrian metamorphic and crystalline basements and were unconformably covered by lower Cambrian, which was deposited in carbonate platform and basinal facies.

(2) These rifting depressions, which were mainly controlled by normal faults, present half-grabens, grabens, and horsts in structural style. They can be divided into three groups with the WNW, ENE, and WNW-trends in the northeastern, central-southern and southwestern parts of the basin, respectively. The main faults began in the Cryogenian, which then inherited activities, and eventually ceased activities at the end of the Ediacaran or in the early Cambrian. The subsidence centres of the rifting depressions migrated eastward along the faults. The fault activities and the development of rifting depressions revealed that the Neoproterozoic Tarim Block was under the tensional NNW-SSE, NNE-SSW trending paleo-stress fields, and was accompanied by clockwise twisting.

(3) The distribution of the main faults and rifting depression groups are coincident with the aeromagnetic anomalies. The transition zone between the southern and the northern rifting depression groupslies at the most prominent high aeromagnetic anomaly zone in the Tarim Basin. Along the main Neoproterozoic faults, there are also the high aeromagnetic anomaly belts, which may reflect strong magmatic activities during the periods of main fault activities. The Neoproterozoic igneous rocks are more developed in the southern and southwestern parts of the basin.

(4) The Cryogenian and Ediacaran fault depressions were mainly in the form of continiental rifts and intra-continental faulted basins. They formed during 0.8–0.61 Ga, and the early rifting was stronger than in later periods. They were a response to the initial opening of the South Altun-West Kunlun and the South Tianshan ocean basins, which reflcts that the Tarim Block and its adjacent areas were wholly in an extensional environment. These rifting depression groups resulted from the break-up of the Supercontinent Rodinia and the initial opening of the proto-Tethys ocean.

Acknowledgements *We are grateful to Academicians Xu Z Q, Zhao W J, and Yang J S for their supports, We thank Professor Qi L X, Wang Z M, Qi J F, Wang Z Q, Yang H J, Qiu H J, Yun L, He D F, He Z L, Yin C M, Li Z J, Bao S J, Sun Z M, and Zhang J X for their help during the study. We are also grateful to two anonymous journal reviewers for their insightful and constructive reviews. We would also like to thank Engineer Zhang M for accurately rendering some of the figures. This study was supported by the National Natural Science Foundation of China (Grant Nos. 41872121 & 41630207), the Basic Scientific Research Projects of the Chinese Academy of Geological Sciences (Grant Nos. JYYWF20180903 & JYYWF20182103), the Science Research project from the Northwest Subsidiary of SINOPEC (Grant No. KY2013-S-024) and the work project of Chinese Geological Survey (Grant Nos. 12120115002101, DD20160022, DD20160169 & 12120115026901).*

References

Allen P A, Armitage J J. 2012. Cratonic basins. In: Busby C, Azor A, eds. Chapter 30 of Tectonics of Sedimentary Basins: Recent Advances. London: Blackwell Publishing Ltd. 602–620

Bureau of Geology and Mineral Resources of Xinjiang Uygur Autonomous Region. 1993. Regional Geology of Xinjiang Uygur Autonomous Region (in Chinese). Beijing: Geological Publishing House. 562

Che Z C, Sun Y. 1996. The age of the Altun granulite facies complex and the basement of the Tarim Basin (in Chinese). Regional Geol China, 15: 51–57

Deng X L, Shu L S, Zhu W B, Ma D S, Wang B. 2008. Precambrian tectonism, magmatism, deformation and geochronology of igneous rocks in the Xingdi fault zone, Xinjiang (in Chinese). Acta Petrol Sin, 24: 2800–2808

Gao L Z, Guo X P, Ding X Z, Gao Z J, Zhang C H, Wang Z Q. 2013. Nanhuan Glaciation Event and Its Stratigraphic Correlation in Tarim Plate, China (in Chinese). Acta Geosci Sin, 34: 39–57

Gao L Z, Wang Z Q, Xu Z Q, Yang J S, Zhang W. 2010. A new evidence from zircon SHRIMP U-Pb dating of the Neoproterozoic diamictite in Quruqtagh area, Tarim basin, Xinjiang, China (in Chinese). Geol Bull China, 29: 205–213

Gao Z J, Chen J B, Lu S N. 1993. Pre-Cambrian System of Northern Xinjiang, No. 6 Pre-Cambrian Geology (in Chinese). Beijing: Geology Press. 171

Gao Z J, Zhu C S. 1984. Pre-Cambrian Geology in Xinjiang China (in Chinese). Urumqi: Xinjiang People's Publishing House. 45

Ge R F, Zhu W B, Zheng B H, Wu H L, He J W, Zhu X Q. 2012. Early Pan-African magmatism in the Tarim Craton: Insights from zircon U-Pb-Lu-Hf isotope and geochemistry of granitoids in the Korla area, NW China. Precambrian Res, 212-213: 117–138

Ge R F, Zhu W B, Wu L, Zheng B H, He J W. 2013. Timing and mechanisms of multiple episodes of migmatization in the Korla complex, northern Tarim Craton, NW China: Constraints from zircon U-Pb-Lu-Hf isotopes and implications for crustal growth. Precambrian Res, 231: 136–156

Gehrels G E, Yin A, Wang X F. 2003a. Magmatic history of the northeastern Tibetan Plateau. J Geophys Res, 108: 2423

Gehrels G E, Yin A, Wang X F. 2003b. Detrital-zircon geochronology of the northeastern Tibetan plateau. Geol Soc Am Bull, 115: 881–896

Guiraud R, Bosworth W, Thierry J, Delplanque A. 2005. Phanerozoic geological evolution of Northern and Central Africa: An overview. J African Earth Sci, 43: 83–143

Guo Z J, Yin A, Robinson A, Jia C Z. 2005. Geochronology and geochemistry of deep-drill-core samples from the basement of the central Tarim basin. J Asian Earth Sci, 25: 45–56

Guo Z J, Zhang Z C, Jia C Z. 2001. Tectonics of Precambrian basement of

the Tarim craton. Sci China Ser D-Earth Sci, 44: 229–236
Guo Z J, Zhang Z C, Wang J J. 1999. Sm-Nd isochron age of ophiolite along northern margin of Altun Tagh Mountain and its tectonic significance. Chin Sci Bull, 44: 456–458
He B Z, Jiao C L, Xu Z Q, Cai Z H, Zhang J X, Liu S L, Li H B, Chen W W, Yu Z Y. 2016. The paleotectonic and paleogeography reconstructions of the Tarim Basin and its adjacent areas (NW China) during the late Early and Middle Paleozoic. Gondwana Res, 30: 191–206
He B Z. 2009. Tectonism and Their Impacts on Hydrocarbon Accumulation in Tarim Basin (in Chinese). Post-Doctor Research Report. Beijing: China Academy of Geological Sciences. 185
He B Z, Jiao C L, Cai Z H, Zhang M, Gao A R. 2011. A new interpretation of the high aeromagnetic anomaly zone in central Tarim Basin (in Chinese with English Abstract). Geol China, 38: 961–965
He D F, Li D S. 1996. Structural Evolution and Hydrocarbon Accumulation in Tarim Basin (in Chinese). Beijing: Geological Publishing House. 56
He D F, Yuan H, Li D, Lei G L, Fan C, Chang Q S, Ye M L. 2011. Chronology, geochemistry and tectonic setting of granites at the core of Tugerming anticline, Tarim Basin: Indications of Paleozoic extensional and compression cycle at the northern margin of Tarim continental block (in Chinese with English Abstract). Acta Petrol Sin, 27: 133–146
He X B, Xu B, Yuan Z Y. 2007. Carbon isotope composition and correlation of Late Neoproterozoic strata in Keping Region, Xinjiang (in Chinese). Chin Sci Bull, 52: 107–113
He Z Y, Zhang Z M, Zong K Q, Wang W, Santosh M. 2012. Neoproterozoic granulites from the northeastern margin of the Tarim Craton: Petrology, zircon U-Pb ages and implications for the Rodinia assembly. Precambrian Res, 212-213: 21–33
He J W, Zhu W B, Ge R F, Zheng B H, Wu H L. 2014. Detrital zircon U-Pb ages and Hf isotopes of Neoproterozoic strata in the Aksu area, northwestern Tarim Craton: Implications for supercontinent reconstruction and crustal evolution. Precambrian Res, 254: 194–209
Hou Z Z, Yang W C. 2011. Multi-scale inversion of density structure from gravity anomalies in Tarim Basin. Sci China Earth Sci, 54: 399–409
Hu A Q, Wei G J. 2006. On the age of the Neoarchean Qingir gray gneisses from the northern Tarim Basin, Xinjiang, China (in Chinese with English Abstract). Acta Geol Sin, 80: 126–133
Hu A Q, Wei G J, Jiang B M, Zhang J B, Deng W F, Chen L L. 2010. Formation of the 0.9 Ga Neoproterozoic granitoids in the Tianshan Orogen, NW China: Constraints from the SHRIMP zircon age determination and its tectonic significance (in Chinese with English Abstract). Geochimica, 39: 197–212
Huang T Z. 2014. Structural interpretation and petroleum exploration targets in northern slope of middle Tarim Basin (in Chinese with English Abstract). Petrol Geol Experi, 36: 257–267
Ingersoll R V. 2012. Tectonics of sedimentary basins, with revised nomenclature. In: Cathy B, Antonio Azor Pe´rez, eds. Tectonics of Sedimentary Basins: Recent Advances. Blackwell Publishing Ltd. 3–43
Jia C Z. 1997. Tectonic Characteristics and Petroleum Tarim Basin China (in Chinese). Beijing: Petroleum Industry Press. 165
Jia C Z. 2004. Petroleum Geology and Exploration of Tarim Basin-Tectonic and Continental Dynamics of Tarim Basin (in Chinese). Beijing: Petroleum Industry Press. 202
Jia C Z. 2009. The structures of basin and range system around the Tibetan Plateau and the distribution of oil and gas in the Tarim Basin (in Chinese with English Abstract). Geotect Metallogen, 33: 1–9
Jia C Z, Zhang S B, Wu S Z. 2004. Stratigraphy of the Tarim Basin and Adjacent Areas (in Chinese). Beijing: Science Press. 516
Jiao F Z. 2017. Significance of oil and gas exploration in NE strike-slip fault belts in Shuntuoguole area of Tarim Basin (in Chinese with English Abstract). Oil Gas Geol, 38: 831–839
Kang J W, Mou C L, Zhou K K, Wang Q Y, Chen X W, Liang W, Ge X Y. 2016. Sequence stratigraphic analysis of the Sinian strata in the Aksu region, Xinjiang (in Chinese with English Abstract). Sediment Geol Tethyan Geol, 36: 47–54
Kang Y Z. 2012. Regularities of oil and gas distribution in China's three major types of basins (in Chinese). Xinjiang Petrol Geol, 33: 635–636
Li H M, Lu S N, Zheng J K, Yu H F, Zhao F Q, Li H K, Zuo Y C. 2001. Dating of 3.6 Ga zircons in granite-gneiss from the eastern Altyn Mountains and its geological significance (in Chinese). Bull Mineral Petrol Geochemi, 20: 259–262
Li J Y, Jia C Z, Hu S L, Huang Z B, Zeng Q, Tan Z J. 1999. The ^{40}Ar-^{39}Ar isotopic age of Wajilitag gabbro in Tarim basin and its geological significance (in Chinese). Acta Petrol Sin, 15: 594–599
Li S Z, Zhao S J, Liu X, Cao H H, Yu S, Li X Y, Somerville I, Yu S Y, Suo Y H. 2018. Closure of the Proto-Tethys Ocean and Early Paleozoic amalgamation of microcontinental blocks in East Asia. Earth-Sci Rev, 186: 37–75
Li Y J, Song W J, Wu G Y, Wang Y F, Li Y P, Zheng D M. 2005. Jinning granodiorite and diorite deeply concealed in the central Tarim Basin. Sci China Ser D-Earth Sci, 48: 2061
Li Y J, Sun D L, Hu S L, Song W J, Wang G L, Tan Z J. 2003. ^{40}Ar-^{39}Ar geochronology of the granite and diorite revealed at the bottom of Tacan 1, the deepest well in China (in Chinese). Acta Petrol Sin, 19: 530–536
Li Y J, Wu G Y, Meng Q L, Yang H J, Han J F, Li X S, Dong L S. 2008. Fault system in central area of the Tarim Basin geometry kinematics and dynamic settings (in Chinese). Chinese J Geol, 43: 82-118
Li Z X, Evans D A D, Halverson G P. 2013. Neoproterozoic glaciations in a revised global palaeogeography from the breakup of Rodinia to the assembly of Gondwanaland. Sediment Geol, 294: 219–232
Li Z X, Bogdanova S V, Collins A S, Davidson A, De Waele B, Ernst R E, Fitzsimons I C W, Fuck R A, Gladkochub D P, Jacobs J, Karlstrom K E, Lu S, Natapov L M, Pease V, Pisarevsky S A, Thrane K, Vernikovsky V. 2008. Assembly, configuration, and break-up history of Rodinia: A synthesis. Precambrian Res, 160: 179–210
Li Z X, Li X H, Kinny P D, Wang J, Zhang S, Zhou H. 2003. Geochronology of Neoproterozoic syn-rift magmatism in the Yangtze Craton, South China and correlations with other continents: Evidence for a mantle superplume that broke up Rodinia. Precambrian Res, 122: 85–109
Li Z X, Zhong S. 2009. Supercontinent-superplume coupling, true polar wander and plume mobility: Plate dominance in whole-mantle tectonics. Phys Earth Planet Inter, 176: 143–156
Liu H F, Li X Q, Liu L Q, Hou G W, Bian H J. 2005. Petroleum plays in rift basins and extensional structures (in Chinese). Oil Gas Geol, 26: 537–552
Liu L, Wang C, Cao Y T, Chen D L, Kang L, Yang W Q, Zhu X H. 2012. Geochronology of multi-stage metamorphic events: Constraints on episodic zircon growth from the UHP eclogite in the South Altyn, NW China. Lithos, 136-139: 10–26
Long X P, Yuan C, Sun M, Kroner A, Zhao G C, Wilde S, Hu A Q. 2011. Reworking of the Tarim Craton by underplating of mantle plume-derived magmas: Evidence from Neoproterozoic granitoids in the Kuluketage area, NW China. Precambrian Res, 187: 1–14
Long X P, Yuan C, Sun M, Zhao G C, Xiao W J, Wang Y J, Yang Y H, Hu A Q. 2010. Archean crustal evolution of the northern Tarim craton, NW China: Zircon U-Pb and Hf isotopic constraints. Precambrian Res, 180: 272–284
Lu S N, Li H K, Zhang C L, Niu G H. 2008. Geological and geochronological evidence for the Precambrian evolution of the Tarim craton and surrounding continental fragments. Precambrian Res, 160: 94–107
Lu S N, Yu H F, Li H K, Guo K Y, Wang H C, Jin W, Zhang C L, Liu Y S. 2006. Study on the Major Geological Problems of the Precambrian Period in China—The Key Geological Event Group and its Global Tectonic Significance of the Precambrian Period in Western China (in Chinese). Beijing: Geological Publishing House. 197
Lu S N, Yuan G B. 2003. Geochronology of early Precambrian magmatic activities in Aketashitage, east Altyn Tagh (in Chinese). Acta Geol Sin, 77: 61–68
Luo J H, Lei G L, Liu L, Xiao Z Y, Wei H X, Che Z C. 2009. The controlling of Altyn structural belt on petroleum geology of the southeastern part of the Tarim Basin, NW China (in Chinese). Geotect Metal, 33: 76–85
Luo Z W, Xu B, He J Y. 2016. U-Pb Detrital Zircon Age Constraints on the

Neoproterozoic Tereeken Glaciation in the Quruqtagh Area, Northwestern China (in Chinese). Acta Sci Natural U Pekinensis, 52: 467–474
Nakajima T, Maruyama S, Uchiumi S, Liou J G, Wang X, Xiao X, Graham S A. 1990. Evidence for late Proterozoic subduction from 700-Myr-old blueschists in China. Nature, 346: 263–265
Persaud P, Tan E, Contreras J, Lavier L. 2017. A bottom-driven mechanism for distributed faulting in the Gulf of California rift. Tectonophysics, 719-720: 51–65
Powell C M A, Preiss W V, Gatehouse C G, Krapez B, Li Z X. 1994. South Australian record of a Rodinian epicontinental basin and its mid-neoproterozoic breakup (~700 Ma) to form the Palaeo-Pacific Ocean. Tectonophysics, 237: 113–140
Qian Y X, Du Y M, Chen D Z, You D H, Zhang J T, Chen Y, Liu Z B. 2014. Stratigraphic sequences and sedimentary facies of Qigebulak Formation at Xianerbulak, Tarim Basin (in Chinese). Petrol Geol Experi, 36: 1–8
Ren JY, Hu D S, Yang H Z, Ying X Y, Li P. 2011.Fault system and its control of carbonate platform in Tazhong uplift area, Tarim basin (in Chinese). China Geol, 38: 935–944
Rogers J J W, Santosh M. 2002. Configuration of Columbia, a Mesoproterozoic supercontinent. Gondwana Res, 5: 5–22
Safonova I Y, Simonov V A, Buslov M M, Ota T, Maruyama S. 2008. Neoproterozoic basalts of the Paleo-Asian Ocean (Kurai accretionary zone, Gorny Altai, Russia): Geochemistry, petrogenesis, and geodynamics. Rus Geol Geophys, 49: 254–271
Safonova I Y, Santosh M. 2014. Accretionary complexes in the Asia-Pacific region: Tracing archives of ocean plate stratigraphy and tracking mantle plumes. Gondwana Res, 25: 126–158
Santosh M, Maruyama S, Yamamoto S. 2009. The making and breaking of supercontinents: Some speculations based on superplumes, super downwelling and the role of tectosphere. Gondwana Res, 15: 324–341
Shu L S, Deng X L, Zhu W B, Ma D S, Xiao W J. 2011. Precambrian tectonic evolution of the Tarim Block, NW China: New geochronological insights from the Quruqtagh domain. J Asian Earth Sci, 42: 774–790
Song S G, Su L, Li X H, Zhang G B, Niu Y L, Zhang L F. 2010. Tracing the 850-Ma continental flood basalts from a piece of subducted continental crust in the North Qaidam UHPM belt, NW China. Precambrian Res, 183: 805–816
Tang L J, Jia C Z. 2007. Structural Analysis and Stress Field Analysis of Tarim Superimposed Basin (in Chinese). Beijing: Science Press. 149
Wang B, Shu L S, Liu H S, Gong H J, Ma Y Z, Mu L X, Zhong L L. 2014. First evidence for ca. 780 Ma intra-plate magmatism and its implications for Neoproterozoic rifting of the North Yili Block and tectonic origin of the continental blocks in SW of Central Asia. Precambrian Res, 254: 258–272
Wang C, Liu L, Che Z C, Chen D L, Zhang A D, Luo J H. 2006. U-Pb geochronology and tectonic setting of the granitic gneiss in Jianggaleisayi eclogite belt, the southern edge of Altyn Tagh (in Chinese). Geol J China U, 12: 74–82
Wang C, Liu L, Yang W Q, Zhu X H, Cao Y T, Kang L, Chen S F, Li R S, He S P. 2013. Provenance and ages of the Altyn Complex in Altyn Tagh: Implications for the early Neoproterozoic evolution of northwestern China. Precambrian Res, 230: 193–208
Wang F T, Song Z Q, Wu S Z. 2006. The Palaeogeographic and Geo-Ecological Atlas of Xinjiang Uygur Autonomous Region Eng (in Chinese). Beijing: Geological Publishing House. 80
Wang F, Wang B, Shu L S. 2010. Continental tholeiitic basalt of the Akesu area (NW China) and its implication for the Neoproterozoic rifting in the northern Tarim (in Chinese). Acta Petrol Sin, 26: 547–558
Wang Y C, Yang H, Wang X M, Zheng B Q. 1994. Takelamakan pre-Sinian paleorift and its petroleum potential (in Chinese). Xinjiang Petro Geol, 15: 191–200
Wei Y F, Li J B, Du H X, Deng Z J, Kang J W. 2010. The significance of the Sinian post-collision peraluminous granites around south margin of the southwest Tianshan (in Chinese). Xinjiang Geol, 28: 242–246
Wu G H, Zhang C Z, Wang H, Liu Y K, Li J J. 2009. Zircon SHRIMP U-Pb age of granodiorite of the Tacan 1 well in the central, Tarim basin, China (in Chinese). Geol Bull China, 28: 568–571
Wu G H, Chen Z Y, Qu T L, Xu Y L, Zhang C Z. 2012. SHRIMP zircon age of the high aeromagnetic anomaly zone in central Tarim Basin and its geological implications. Natural Sci, 4: 1–4
Wu G Y, Li Y J, Wang G L, Zheng W, Luo J C, Meng Q L. 2006. Volcanic rocks of Jinningian oceanic islands in the Bachu area, Western Xinjiang (in Chinese). Geoscience, 20: 361–369
Wu L, Guan S W, Ren R, Wang X B, Yang H J, Jin J Q, Zhu G Y. 2016. The characteristics of Precambrian sedimentary basin and the distribution of deep source rock: A case study of Tarim Basin in Neoproterozoic and source rocks in Early Cambrian, Western China (in Chinese). Petrole Explor Develop, 43: 905–915
Xiao X C, Tang Y Q, Li J T, Feng Y M, Zhu B Q. 1990. Geotectonic Evolution in Northern Xinjiang (in Chinese). Xinjiang Geol Sci, 1: 47–68
Xu B R. 1997. Basement rock distribution in Tarim Basin Inferred from aeromagnetic data (in Chinese). J Xi'an Petro Inst, 12: 8–11
Xu B, Jiang P, Zheng H F, Zou H B, Zhang L F, Liu D Y. 2005. U-Pb zircon geochronology and geochemistry of Neoproterozoic volcanic rocks in the Tarim Block of northwest China: Implications for the breakup of Rodinia supercontinent and Neoproterozoic glaciations. Precambrian Res, 136: 107–123
Xu B, Kou X W, Song B, We W, Wang Y. 2008. SHRIMP dating of the upper Proterozoic volcanic rocks in the Tarim plate and constraints on the Neoproterozoic glaciation (in Chinese). Acta Petrol Sin, 24: 2857–2862
Xu B, Xiao S H, Zou H B, Chen Y, Li Z X, Song B, Liu D Y, Zhou C M, Yuan X L. 2009. SHRIMP zircon U-Pb age constraints on Neoproterozoic Quruqtagh diamictites in NW China. Precambrian Res, 168: 247–258
Xu B, Zou H B, Chen Y, He J, Wang Y. 2013. The Sugetbrak basalts from northwestern Tarim Block of northwest China: Geochronology, geochemistry and implications for Rodinia breakup and ice age in the Late Neoproterozoic. Precambrian Res, 236: 214–226
Xu Z Q, He B Z, Zhang C L, Zhang J X, Wang Z M, Cai Z H. 2013. Tectonic framework and crustal evolution of the Precambrian basement of the Tarim Block in NW China: New geochronological evidence from deep drilling samples. Precambrian Res, 235: 150–162
Xu Z Q, Li S T, Zhang J X, Yang J S, He B Z, Li H B, Lin C S, Cai Z H. 2011. Paleo-Asian and Tethyan tectonic systems with docking the Tarim block (in Chinese). Acta Petrol Sin, 27: 1–22
Yong W J, Zhang L F, Hall C M, Mukasa S B, Essene E J. 2013. The $^{40}Ar/^{39}Ar$ and Rb-Sr chronology of the Precambrian Aksu blueschists in western China. J Asian Earth Sci, 63: 197–205
Yan L, Li M, Pan W Q. 2014. Distribution characteristics of Permian igneous rock in Tarim basin-based on the high-precision aeromagnetic data (in Chinese). Progress Geophys, 29: 1843–1848
Yang S F, Chen L F, Xiao Z R, Luo J C, Chen H L, Wang B Q, Chen X G, Liao L. 2009. The Cenozoic fault system of southeastern Tarim basin (in Chinese). Geotectonic Metall, 33: 33–37
Yang W C, Wang J L, Zhong H Z, Chen B. 2012. Analysis of regional magnetic field and source structure in Tarim Basin (in Chinese). Chinese J Geophys, 55:1278–1287
Yin X H, Li Y S, Liu Z P. 1998. Gravity field and crust-upper mantle structure over the Tarim Basin (in Chinese). Seismol Geol. 20: 370–378
Yuan X C. 1996. Atlas of Geophysics in China (in Chinese). Beijing: Geological Pubblishing House. 200
Zhai M G, Santosh M. 2011. The early Precambrian odyssey of the North China Craton: A synoptic overview. Gondwana Res, 20: 6–25
Zhang C L, Li H K, Wang H Y. 2012b. A Review on Precambrian tectonic evolution of Tarim block: Possibility of interaction between Neoproterozoic plate subduction and mantle plume (in Chinese). Geol Rev, 58: 923–936
Zhang C L, Li X H, Li Z X, Lu S N, Ye H M, Li H M. 2007a. Neoproterozoic ultramafic–mafic-carbonatite complex and granitoids in Qur-

uqtagh of northeastern Tarim Block, western China: Geochronology, geochemistry and tectonic implications. Precambrian Res, 152: 149–169
Zhang C L, Li Z X, Li X H, Ye H, Wang A, Guo K Y. 2006. Neoproterozoic bimodal intrusive complex in the Southwestern Tarim Block, Northwest China: Age, geochemistry, and implications for the rifting of Rodinia. Int Geol Rev, 48: 112–128
Zhang C L, Li Z X, Li X H, Yu H F, Ye H M. 2007b. An early Paleoproterozoic high-K intrusive complex in southwestern Tarim Block, NW China: Age, geochemistry, and tectonic implications. Gondwana Res, 12: 101–112
Zhang C L, Li Z X, Li X H, Ye H M. 2009. Neoproterozoic mafic dyke swarms at the northern margin of the Tarim Block, NW China: Age, geochemistry, petrogenesis and tectonic implications. J Asian Earth Sci, 35: 167–179
Zhang C L, Yang D S, Wang H Y, Dong Y G, Ye H M. 2010. Neoproterozoic mafic dykes and basalts in the southern margin of Tarim, Northwest China: Age, geochemistry and geodynamic implications. Acta Geol Sin-Engl Ed, 84: 549–562
Zhang C L, Ye X T, Zou H B, Chen X Y. 2016. Neoproterozoic sedimentary basin evolution in southwestern Tarim, NW China: New evidence from field observations, detrital zircon U-Pb ages and Hf isotope compositions. Precambrian Res, 280: 31–45
Zhang C L, Zhao Y, Guo K Y, Dong Y G, Wang A G. 2003. Geochemistry characteristics of the Proterozoic meta-basalt in Southern Tarim Plate: Evidence for the Mesoproterozoic breakup of Paleo-Tarim Plate (in Chinese). Earth Sci J China U Geosci, 28: 47–53
Zhang C L, Zou H B, Wang H Y, Li H K, Ye H M. 2012a. Multiple phases of the Neoproterozoic igneous activity in Quruqtagh of the northeastern Tarim Block, NW China: Interaction between plate subduction and mantle plume? Precambrian Res, 222-223: 488–502
Zhang J X, Gong J H, Yu S Y. 2012. c.1.85 Ga HP granulite-facies metamorphism in the Dunhuang block of the Tarim Craton, NW China: Evidence from U-Pb zircon dating of mafic granulites. J Geol Soc, 169: 511–514
Zhang C L. Lu S N, Yu H F, Ye H M. 2007c. Tectonic evolution of the Western Kunlun orogenic belt in northern Qinghai-Tibet Plateau: Evidence from zircon SHRIMP and LA-ICP-MS U-Pb geochronology. Sci China Ser D-Earth Sci, 50: 825–835
Zhang G Y, Liu W, Zhang L, Yu B S, Zhang B M, Wang L D. 2015. Cambrian-Ordovician prototypic basin, paleogeography and petroleum of Tarim Craton (in Chinese). Earth Sci Front, 22: 269–276
Zhang J X, Li H K, Meng F C, Xiang Z Q, Yu S Y, Li J P. 2011. Polyphases tectonothermal events recorded in “metamorphic basement” from the Altyn Tagh, the southeastern margin of the Tarim basin, western China: Constraint from U-Pb zircon geochronology (in Chinese). Acta Petrol Sin, 27: 23–46
Zhang J X, Mattinson C G, Meng F C, Wan Y S. 2005a. An Early Palaeozoic HP/HT granulite-garnet peridotite association in the south Altyn Tagh, NW China: *P-T* history and U-Pb geochronology. J Metamorph Geol, 23: 491–510
Zhang J X, Meng F C, Yu S Y, Chen W, Chen S Y. 2007. ^{39}Ar-^{40}Ar geochronology of high-pressure/low-temperature blueschist and eclogite in the North Altyn Tagh and their tectonic implications (in Chinese). Geol China, 34: 558–564
Zhang J X, Yang J S, Mattinson C G, Xu Z Q, Meng F C, Shi R D. 2005b. Two contrasting eclogite cooling histories, North Qaidam HP/UHP terrane, western China: Petrological and isotopic constraints. Lithos, 84: 51–76
Zhang J X, Yu S Y, Gong J H, Li H K, Hou K J. 2013. The latest Neoarchean-Paleoproterozoic evolution of the Dunhuang block, eastern Tarim craton, northwestern China: Evidence from zircon U-Pb dating and Hf isotopic analyses. Precambrian Res, 226: 21–42
Zhang J X, Yu S Y, Li Y S, Yu X X, Lin Y H, Mao X H. 2015. Subduction, accretion and closure of Proto-Tethyan Ocean: Early Paleozoic accretion/collision orogeny in the Altun-Qilian-North Qaidam orogenic system (in Chinese). Acta Petrol Sin, 31: 3531–3554
Zhang Y L, Wang Z Q, Yan Z, Wang T. 2013. Neoproterozoic volcanic rocks in the Southern Quruqtagh of Northwest China: Geochemistry, zircon geochronology and tectonic implications. Acta Geol Sin-Engl Ed, 87: 118–130
Zhang Z C, Kang J L, Kusky T, Santosh M, Huang H, Zhang D Y, Zhu J. 2012. Geochronology, geochemistry and petrogenesis of Neoproterozoic basalts from Sugetbrak, northwest Tarim block, China: Implications for the onset of Rodinia supercontinent breakup. Precambrian Res, 220-221: 158–176
Zhao G C, Cawood P A. 2012. Precambrian geology of China. Precambrian Res, 222-223: 13–54
Zhao G C, Cawood P A, Wilde S A, Sun M. 2002. Review of global 2.1–1.8 Ga orogens: Implications for a pre-Rodinia supercontinent. Earth-Sci Rev, 59: 125–162
Zhao G C, Sun M, Wilde S A, Li S Z. 2004. A Paleo-Mesoproterozoic supercontinent: Assembly, growth and breakup. Earth-Sci Rev, 67: 91–123
Zhao J M, Cheng H G, Pei S P, Liu H B, Zhang J S, Liu B F. 2008. Deep structure of north margin of Tarim Basin (in Chinese). Chinese Sci Bull, 53: 946–955
Zheng B H, Zhu W B, Shu L S, Zhang Z Y, Yu J J, Huang W T. 2008. The protolith of the Aksu Precambrian blueschist and its tectonic setting (in Chinese). Acta Petrol Sin, 24: 2839–2848
Zhou X B, Li J H, Wang H H, Li W S, Cheng Y L. 2015. The type of prototypic basin and tectonic setting of Tarim Basin formation from Nanhua to Sinian (in Chinese). Earth Sci Front, 22: 290–298
Zhu W B, Ge R F, Shu L S Zheng B H. 2017. Tectonic-Magmatic Events and Crustal Evolution of Precambrian in the North Margin of Tarim Craton (in Chinese). Beijing: Science Press. 437
Zhu W B, Zhang Z Z, Shu L S, Lu H F, Sun J B, Yang W. 2008. SHRIMP U-Pb zircon geochronology of Neoproterozoic Korla mafic dykes in the northern Tarim Block, NW China: Implications for the long-lasting breakup process of Rodinia. J Geol Soc, 165: 887–890
Zhu W B, Zheng B, Shu L, Ma D, Wu H, Li Y, Huang W, Yu J. 2011. Neoproterozoic tectonic evolution of the Precambrian Aksu blueschist terrane, northwestern Tarim, China: Insights from LA-ICP-MS zircon U-Pb ages and geochemical data. Precambrian Res, 185: 215–230
Zong W M, Gao L Z, Ding X Z, Pang W H. 2010. Characteristics of Nanhuan diamictite (tillite) and stratigraphic correlation in the southwestern margin of Tarim Basin (in Chinese). Geol China, 37: 1183–1190

(Responsible editor: Shaofeng LIU)